NASA-CR-192635

INSTITUTE FOR ASTRONOMY
UNIVERSITY OF HAWAII
2680 WOODLAWN DRIVE
HONOLULU HAWAII 96822

FINAL REPORT

FOR

NATIONAL AERONAUTICS AND SPACE ADMINISTRATION

GRANT NAG 5-1823

STELLAR LYMAN ALPHA EMISSION AND THE LOCAL INTERSTELLAR MEDIUM

(NASA-CR-192635) STELLAR LYMAN ALPHA EMISSION AND THE LOCAL INTERSTELLAR MEDIUM Final Technical Report, 15 Nov. 1991 - 14 Nov. 1992 (Hawaii Univ.) 50 p

N93-22381

Unclas

G3/89 0151380

PRINCIPAL INVESTIGATOR: DR. THEODORE SIMON

1991 NOVEMBER 15 - 1992 NOVEMBER 14

I. Scope of Work

Under the auspices of this *ADP* program, a systematic study has been made of *IUE* archival images in order to extract spectra of the Lyman α region and to measure the stellar Lyman α flux for as many late-type stars as possible. The Lyman α resonance line is a powerful cooling channel for the hot chromospheres of solar-type stars, but has not been studied before in any systematic fashion across the H-R diagram. A major deterrent which has limited the use of Lyman α in the study of stellar chromospheres is the contamination of this spectral feature caused by the scattering of solar Lyman α photons in the Earth's exosphere. This scattered light is monochromatically imaged through the entrance slot of the *IUE* telescope and is superposed onto the stellar spectrum. In all but the shortest exposures with *IUE*, this "geocoronal emission" overwhelms the stellar flux and makes it impossible to directly measure the strength of the stellar chromospheric feature. The IUESIPS processing contains no provision for correcting standard G.O. output products for this contamination.

Our first task was to develop a scheme for removing the geocoronal flux, specifically from low-dispersion spectra taken with the Short-Wavelength Camera of *IUE*. The strategy we adopted was to fit a "sky model" to the spatially-resolved geocoronal emission observed through the large science aperture of the telescope, using the spectral orders on either side of the central ones where the stellar emission is concentrated. The model emission was then subtracted from the observed image, leaving behind the corrected stellar Lyman α emission. The details of this fitting procedure are described in the manuscript that accompanies this report.

Having devised a succesful method for removing the unwanted geocoronal emission, we applied our correction procedure to 366 archival images which, from inspection of the photowrites in the *IUE* browse file, seemed especially promising. In this survey, we were eventually able to detect Lyman α emission in the spectra of 227 stars representing a wide range in age, temperature, and luminosity throughout the cool half of the H-R diagram. Previously fewer than 30 such stars had been measured, and so our study provides an order of magnitude increase in the numbers of stars having Lyman α flux measurements. We have made multiple measurements for 52 stars and also derived upper limits on chromospheric flux for another 48 stars.

II. Major Scientific Results

In our Lyman α survey, we have found more than a dozen late A and early F main sequence stars with chromospheric emission, showing that stars with very shallow convection zones can energize chromospheres much more powerful than the Sun's. This is not a result that was anticipated prior to *IUE*, that is, before we had the means of routinely exploring the far UV spectra of so many different classes of stars. It is one that has important implications for our understanding of stellar dynamos and of the physical processes believed to be responsible for outer atmospheric heating. For a subset of 149 stars in our sample, we were also able to make a further correction for the attenuation caused by the local interstellar medium and thus to derive the intrinsic stellar Lyman α flux. Based on this collection of fluxes, we have established empirical correlations between the strength of Lyman α and coronal X ray emission. Theoretical studies of these trends using stellar atmospheres and NLTE radiative transfer models should now provide a better understanding of how Lyman α is formed, of the structure of stellar chromospheres, and of the mechanisms by which chromospheres are heated for a wide range of different types of stars, including the Sun.

Our measurements -- just the detection of so many different stars -- also demonstrate that interstellar H I column densities along many lines of sight in the neighborhood of the Sun

are exceedingly low, so that many potential sources of EUV emission should be detectable by spacecraft working at wavelengths below Lyman α. The EUV region is one of the last remaining spectral windows through which astronomers have had few glimpses of the sky.

III. Papers Submitted for Publication

The following paper was submitted for publication and is now scheduled to appear in the 1993 May 1 issue of The Astrophysical Journal: "A Catalog of Stellar Lyman Alpha Fluxes," by Wayne Landsman and Theodore Simon. A copy of the manuscript accepted for publication is attached.

A Catalog of Stellar Lyman Alpha Fluxes

Wayne Landsman
Hughes /STX, NASA/GSFC
Code 681, Greenbelt, MD 20771

Theodore Simon[1]
Institute for Astronomy, University of Hawai'i

To appear in the 1993 May 1 issue of
The Astrophysical Journal

[1]Guest Observer with the *International Ultraviolet Explorer* (*IUE*) satellite.

Abstract

We present a catalog of stellar Lyα emission fluxes, based on new and archival images obtained with the International Ultraviolet Explorer (IUE) spacecraft. The fluxes have been corrected for the contamination caused by diffusely scattered solar Lyα by means of an extraction procedure that utilizes spatial information perpendicular to the dispersion direction in the IUE line-by-line images. The catalog includes 227 stars with detectable Lyα emission fluxes, and upper limits on the Lyα emission flux for another 48 stars. Multiple flux measurements are given for 52 stars. We present a model for correcting the observed Lyα flux for attenuation by the local interstellar medium, and we apply this model to derive intrinsic Lyα fluxes for 149 catalog stars which are located in low H I column density directions of the local interstellar medium.

In our catalog, there are 14 late A and early F stars at B–V $\leq$ 0.29 that show detectable emission at Lyα. We find a linear correlation between the intrinsic Lyα flux and C II 1335 Å flux for stars with B–V $>$ 0.60, but the A and F stars deviate from this relation in the sense that their Lyα flux is too low. We also find a good correlation between Lyα strength and coronal X-ray emission. This correlation holds over most of the H-R diagram, even for the F stars, where an X-ray deficit has previously been found relative to the transition region lines of C II and C IV.

Subject headings: stars:chromospheres — ultraviolet:stars – ultraviolet: interstellar

1 Introduction

The Lyα line of neutral hydrogen is generally the brightest emission line in the far-ultraviolet spectra of late-type stars. There have been extensive studies of Lyα in the Sun (e.g., Fontenla, Reichman & Tandberg-Hanssen 1988), where its integrated flux is equivalent to the total solar emission at all wavelengths less than 1500 Å. Lyα directly or indirectly influences the way in which numerous other UV lines in the solar atmosphere are formed, and the sharp rise from chromospheric to coronal temperatures is due in large part to the loss of neutral hydrogen as an efficient cooling channel. In the case of other late-type stars, however, Lyα has been little studied, despite the fact that this line is routinely exposed during every observation with the short wavelength (SWP) camera of the IUE spacecraft.

There are two reasons for this relative neglect of the Lyα line in studies of stellar chromospheres. The first is that the observations are contaminated by diffuse emission due to solar Lyα, which is resonantly scattered by neutral hydrogen (H I) in the Earth's geocorona and in the interplanetary medium. Yet, as a number of authors have realized (Clarke *et al.* 1986; Rucinski, Vilhu, & Whelan 1985; Byrne & Doyle 1989), it is fairly straightforward to correct for this diffuse Lyα emission in IUE low-dispersion, large aperture images. The strength of the diffuse Lyα emission can be estimated by utilizing the spatial information in the IUE image perpendicular to the dispersion direction. An appropriately scaled blank sky image can be used to estimate the amount of diffuse Lyα emission which must be subtracted out to leave behind just the stellar Lyα flux.

The second, and more serious, obstacle to stellar Lyα studies is that, even for nearby stars, the intrinsic stellar emission is strongly attenuated by H I in the local interstellar medium (LISM). The LISM is a region of unusually low H I density (Bruhweiler & Vidal-Madjar 1987; Frisch & York 1991), and there appear to be few sightlines within 50 pc of the Sun where the H I column density exceeds 5×10^{18} cm^{-2}. Nevertheless, even a modest H I column density of 5×10^{17} cm^{-2} would be enough to attenuate a Lyα profile like the Sun's by a factor of two. In principle, however, if the properties of the LISM along a line of sight are sufficiently well determined, then it should still be possible to compute an interstellar attenuation factor, and thereby recover the intrinsic Lyα flux of the star. This has been possible for a handful of stars (Neff *et al.* 1986; Linsky *et al.* 1992), where there are high dispersion Lyα observations of sufficient quality to allow modelling of the interstellar medium along the line of sight.

An alternative approach, in the absence of high dispersion spectra, is to to acquire low dispersion Lyα flux measurements of a statistically large number of stars. By comparing

stars at a variety of distances and directions, one should be able to draw conclusions about the behavior of Lyα across the HR diagram, and to obtain flux-flux relations between Lyα and other measures of stellar activity. Conversely, by comparing the Lyα flux of stars with ostensibly similar chromospheric activity levels, one should be able to derive information on the relative H I opacity of the LISM. With these goals in mind, we have undertaken a systematic study of the IUE archives for the purpose of obtaining the Lyα emission flux of as many stars as possible.

This paper presents a catalog of stellar Lyα fluxes based on our analysis of 366 IUE images. In this work, we were able to detect Lyα emission from 227 stars, a number that far exceeded our original expectations. In §2 we discuss the selection of stars in the catalog and give details of our data reduction. The observed Lyα fluxes are presented in §3, and in §4 we construct synthetic Lyα profiles and discuss the parameters that have the strongest influence on the amount of interstellar attenuation. Intrinsic Lyα fluxes are then estimated for 149 stars in the catalog which are at distances and in directions where the properties of the LISM are fairly well understood. Finally, in §5 we survey the behavior of Lyα across the cool half of the HR diagram, compare our Lyα data with other more extensively studied chromospheric and coronal diagnostics. Some results from a preliminary version of this catalog are given in Landsman and Simon (1991).

2 DATA REDUCTION

2.1 Selection of IUE Images

The IUE images used in this study were obtained from both our own programs (e.g., Simon & Landsman 1991) as well as from the IUE archives. Our goal was to identify every late-type stars which shows evidence of Lyα emission in at least one IUE image. We almost certainly missed a few stars, however, because of necessary shortcuts required to process the large amount of archival IUE data.

We began by searching the IUE logs for all low dispersion, large aperture SWP images of late-type stars with exposure times under 100 minutes. We did not include Herbig Ae stars or cataclysmic variables in the search, although extremely broad Lyα emission lines (presumably arising from an acretion disk) have been detected in IUE spectra of several of these stars (Blondel, Talavera, & Tjin A Djie 1992). Multiple and trailed exposures were also excluded because of the difficulty of subtracting out the diffuse Lyα emission from such images. The images with exposure times longer than 100 minutes were excluded from our search because they are nearly always saturated at Lyα by the diffuse sky emission.

To minimize the amount of computer processing involved, we first visually inspected the photowrites of the candidate images that we had picked out in our search of the IUE logs. This inspection was limited to images from Goddard, since we did not have access to the photowrites of images taken at the VILSPA station. An image was selected for further processing if it showed stellar Lyα emission on the photowrite. Images which did not show Lyα emission were also selected for further processing if (1) the star was within 100 pc, and (2) other emission lines, such as C II and C IV were present on the photowrite. This second category of stars was included to identify stars that might be located behind unusually large column densities of H I.

There are 52 stars in our catalog for which we measured the Lyα flux on more than one image. These data can be used to test for variability of the Lyα flux, or to assess the repeatability of our flux measurements. However, the study of Lyα variability was not a major goal of this work, and our search of the IUE archives for multiple images was far from exhaustive. For example, Hallam, Altner, & Endal (1991) measured Lyα fluxes from 20 images of ϵ Eri, and 33 images of α Cen A, in their study of rotational modulation of chromospheric emission lines, whereas in our catalog we include just 6 flux measurements of ϵ Eri and 5 measurements of α Cen A.

The exposure times of many IUE archival SWP images were optimized for detecting weak emission in the chromospheric lines of either C II and C IV, and in these exposures the stronger Lyα feature is often saturated. There are twelve stars in our catalog in which the stellar Lyα feature is saturated on all existing IUE low-dispersion images. For seven of these stars, we have been able to estimate a Lyα flux from archival high-dispersion spectra, as described in §2.3. There remained five stars (α Phe, ζ And, α Ari, γ Phe, and μ UMa) in our catalog which showed strong stellar Lyα emission, but which were saturated all existing IUE high and low dispersion spectra. The saturated flux for these five stars was measured in the normal way but recorded as lower limit.

2.2 Subtraction of Diffuse Lyα

Solar Lyα is scattered into the aperture of the IUE spectrograph by neutral hydrogen in the geocorona and in the interplanetary medium (Fricke and Ojanguren 1980). The natural linewidth of this diffuse emission is much less than the FWHM of the IUE low-dispersion spectrograph, so that its effect is to monochromatically "image" the $10'' \times 21''$ aperture onto the SWP camera. In low dispersion, the major axis of the large aperture is oriented roughly perpendicular to the dispersion direction. The actual strength of the diffuse emission seen by IUE during any observation depends in a complicated way upon look direction, orbital

height, and the time-varying intensity of the solar Lyα flux. However, the instrumental response to a *point* source is only $\sim 5''$ FWHM (Cassatella, Barbero, & Benvenuti 1985), and so the diffuse emission recorded at the outer edges of the large aperture can be used to fit an empirical model of the diffuse emission across the entire entrance slot, including the central spectral orders where the stellar emission is concentrated. An SWP image of the sky background can then be scaled and subtracted to obtain a spectrum containing only stellar emission (see Figure 1).

We utilize the extended line-by-line (ELBL) file which consists of 110 different narrow spectra, extracted in a direction parallel to the dispersion. In the standard IUE point source extraction, lines 47-64 are integrated to obtain a stellar flux, and a background is determined from lines 29-38 and 73-82. In most cases, we determined the diffuse Lyα emission strength by a pixel by pixel least-squares fit of a sky image to the emission in lines 40-45 and 66-71. The actual line numbers used could be modified if the star had not been properly centered in the aperture. In addition to the scale factor, we include as free parameters shifts parallel and perpendicular to the dispersion, and a rotation of the sky image. These free parameters provide adjustments for thermal shifts between the stellar image and the sky background image. Each parameter (scale factor, rotation, and shift) is varied individually to minimize χ^2, and then the process is repeated until changes in the value of χ^2 in successive iterations fall below a preset tolerance level.

Prior to a changeover in the IUESIPS reduction software on 1 October 1985, the standard line-by-line output file was sampled only half as often in the spatial direction for a total of 55 spectra (Muñoz-Piero 1986). Therefore, in our analysis, all of the raw images taken before 1 October 1985 have been reprocessed with the Dean Image Processing System (DIPS, Ahmad 1986), which emulates the standard IUE processing scheme in use in 1986.

The accuracy of the diffuse Lyα subtraction can be judged by the smoothness of the residual profiles both perpendicular and along the dispersion direction. In general, we find that the Lyα subtraction is most successful when the sky image used in the subtraction is taken within a couple of months of the stellar image. This result is consistent with the experience of Clarke *et al.* (1986) who noticed, in their study of the variability of the Lyα emission from Uranus, that the "fixed" noise pattern in the Lyα region of the camera seemed to vary on a timescale of months. Generally, during our own programs, we obtained one sky image during the same shift as the stellar exposures. However, since it proved impractical to obtain a "best" sky image for each of the many archival stellar images that we analyzed, we instead created two "average" sky profiles. The first was derived by coaddition of 10 sky images taken before SWP 29000, and a second one was obtained by coadding 4 sky images

taken after SWP 29000. Sky images taken before SWP 29000 gave poor sky subtraction results when used with more recent images; this effect may be related to the unexplained wavelength shifts which appeared in IUE images at this time (Thompson 1988). The most appropriate averaged sky profile was used to subtract the diffuse Lyα emission from each of our archival stellar images. In the few cases where the use of an average sky emission resulted in large residuals, we attempted to find sky images close in time to the stellar exposure.

The Lyα fluxes are corrected for the time change in the sensitivity of the SWP camera, using the factors given by Bohlin and Grillmair (1988) for large-aperture images, with an unpublished update through 1989.36. The temporal corrections at 1210, 1215 and 1220 Å were averaged together in order to smooth over the large time and wavelength variations which appear in the Bohlin and Grillmair tables near Lyα. The sensitivity at Lyα shows a 15% decrease by the year 1989.36, and we assumed no further sensitivity change for images taken after this time. The Lyα fluxes were also corrected for the small change of camera sensitivity with temperature (Imhoff 1986). The absolute calibration was obtained by spline interpolation in the table of Bohlin *et al.* (1980), which yielded an inverse sensitivity at 1215.7 Å of $S^{-1} = 3.28 \times 10^{-14}$ erg cm^{-2} Å^{-1} s^{-1} (FN s^{-1})$^{-1}$. This factor (and our derived fluxes) would be only 2% smaller if we had instead adopted the absolute calibration of Bohlin *et al.* (1990).

After removing the diffuse Lyα emission, we integrated the line-by-line spectrum in the standard way to form a flux vs. wavelength spectrum. The Lyα fluxes were then measured by integration over a $\sim$ 10 Å interval centered near 1215 Å; in practice, the integration limits were interactively determined for each image. Occasionally, as in the case of β Cas, emission from Si III near 1206 Å is sufficiently strong to blend with the blue wing of the Lyα emission, and cause an additional, but nevertheless minor, uncertainty in the flux determination.

2.3 High-dispersion images

Our reduction of the high-dispersion SWP images differs from the standard IUE processing in three ways: the background subtraction, the removal of the diffuse sky emission, and the absolute calibration. The background level was determined using a flux-free region away from the Lyα emission, since the interorder background can be contaminated by spillover from diffuse geocoronal Lyα. The diffuse sky emission was removed following the procedure outlined by Landsman *et al.* (1984), in which a sky-only spectrum is scaled and subtracted from the stellar spectrum. The scaling factor is determined by the requirement that zero flux remain in the interstellar core of the high-dispersion stellar profile after the subtraction. (In high-dispersion IUE images the large aperture is aligned *along* the disper-

sion direction, and there is very limited information on the strength of the sky emission perpendicular to the dispersion.) One difficulty with our adopted subtraction algorithm is that the high dispersion profile of the diffuse emission may vary with time, in particular, due to velocity shifts between the geocoronal and interplanetary emissions (Clarke *et al.* 1984). The most accurate subtraction of the diffuse Lyα emission will occur when the sky spectrum is taken under similar observing conditions and in a similar direction to the stellar spectrum (Catalano *et al.* 1991), but such ideal sky images are not generally available in the IUE archives. However, we do not expect our use of an average high-dispersion sky-only spectrum will introduce large errors in the net integrated Lyα stellar flux.

Considerable uncertainty still exists concerning the absolute calibration of IUE high-dispersion emission-line fluxes at Lyα. The range of validity of the standard emission line calibration of Cassetella, Ponz, and Selvelli (1983) is from 1400 Å to 1975 Å. Ayres (1988a) tested whether the Cassetella *et al.* calibration could be extrapolated to Lyα by comparing high and low dispersion spectra of Capella obtained during a single IUE shift. He found the high-dispersion Lyα fluxes from the extrapolated Cassetella *et al.* calibration needed to be multiplied by 1.25 (corresponding to a sensitivity factor of $S^{-1} = 10.4 \times 10^{-14}$ ergs cm^{-2} Å^{-1} s^{-1} (FN min^{-1})$^{-1}$) to agree with the low-dispersion fluxes. A limitation of the Ayres study is that the adopted low-dispersion Capella spectra included saturated pixels at Lyα. We adopt a high-dispersion sensitivity factor of $S^{-1} = 11.8 \times 10^{-14}$ ergs cm^{-2} Å^{-1} s^{-1} (FN min^{-1})$^{-1}$ based primarily on our own comparison of high and low dispersion spectra of Procyon. No attempt was made to correct for any time dependence of the sensitivity of the SWP camera at high dispersion.

2.4 Comparison with other subtraction algorithms

Several other algorithms have been described in the literature for the removal of diffuse Lyα emission from low-dispersion IUE images. Catalano *et al.* (1986) fit an ellipsoid to the Lyα feature in the geometrically and photometrically corrected IUE image file. We cannot directly compare their results with ours because we do not know which images they used, and in any case there are only four stars in common. Neff *et al.* (1986) and Vilhu, Neff & Rahunen (1989) use the line-by-line image and model the sky emission with gaussian wings in the outer portion of the aperture, and linear interpolation across the center. We have used their algorithm on several of our images and find reasonable agreement with our own flux determinations.

Byrne and Doyle (1989, 1990) and Doyle, Panagi, & Byrne (1990) have recently published Lyα fluxes or upper limits for 26 M dwarf stars. They model the diffuse Lyα component

by extracting a 1-d spectrum in the line by line image alongside the central star position; they then subtract this sky spectrum from the stellar spectrum. For two stars on their list (Gliese 54.1 and Gliese 900), we find no evidence of Lyα emission, with our upper limits being about equal to their claimed detection levels. There is reasonable agreement for the remaining stars in common, with up to a factor of two discrepancy for some of the fainter fluxes.

Böhm-Vitense and Woods (1983) gave Lyα fluxes for 23 F stars, of which 17 appear in the current study. Their corrections for diffuse emission were derived entirely from the shape of the wings of the 1-D Lyα profile. This procedure should not be as accurate as the methods that make explicit use of spatial information in the line-by-line file, because most of the diffuse emission occurs along the major axis of the large aperture, which lies perpendicular to the dispersion direction. There are four stars (δ Hor, 76 Tau, ξ Her, and θ Cyg) with published fluxes in their paper, for which we found no evidence of stellar emission in the line-by-line image; otherwise their fluxes are in fair (30% mean differences) agreement with ours.

3 Lyman Alpha Catalog

Table 1 lists 366 Lyα flux measurements for 275 stars. The stellar parameters given in the table were obtained from preliminary new editions of the Bright Star Catalog (Hoffleit and Warren 1991) and the Gliese catalog (Gliese and Jahreiss 1991), or the catalog of chromospherically active binary stars (Strassmeier *et al.* 1988). In the last column, we have converted the observed Lyα flux into a normalized flux, R(Lyα), by dividing by the apparent stellar bolometric luminosity. A double colon following a flux value indicates that there was significant noise present in the residuals after the diffuse Lyα emission had been subtracted, or that the flux value was measured from a high dispersion spectrum. A single colon indicates that the correction for diffuse Lyα was large but that the residuals following the subtraction were small. Only for a few of the brightest stars (e.g., Procyon, α Cen A) was the correction for diffuse Lyα emission negligible.

4 Intrinsic Lyα Fluxes

High-dispersion stellar Lyα observations show a broad chromospheric Lyα emission line cut by a saturated interstellar H I absorption feature. The interstellar Lyα attenuation factor – i.e., the factor by which the intrinsic stellar Lyα flux is reduced by interstellar absorption – will depend in detail on both the stellar emission profile and the interstellar absorption

profile. In this section, we estimate the Lyα attenuation factor for a subset of the stars in our catalog, relying on currently known properties of the LISM, and reasonable expectations concerning the appearance of the intrinsic stellar Lyα emission profiles.

Section 4.1 provides a brief summary of high-dispersion studies of solar and stellar Lyα profiles. In §4.2, we construct synthetic profiles, and consider how the Lyα attenuation factor depends on various stellar and interstellar parameters. This section also discusses the Lyα linewidth-luminosity (Wilson-Bappu) relation, which is critical for estimating the interstellar Lyα attenuation factor. Next, in §4.3 we consider the distribution of H I in the solar neighborhood. Based on this information, we estimate the intrinsic Lyα emission flux of 149 stars which appear to be located in directions of low H I column density.

4.1 Solar and Stellar Ly alpha

Solar observations have always been essential to an understanding of stellar chromospheres, because the Sun is the only star whose surface activity can be spatially resolved. Solar data are even more important for Lyα studies, because only in the Sun it is possible to observe the core of a Lyα profile without interference from intervening interstellar H I. Solar Lyα observations are contaminated by gecoronal *absorption* of the line core, but it is possible to model and correct for this absorption, (Fontenla, Reichmann, and Tandberg-Hannsen 1988).

The spatially integrated Lyα flux from the Sun can vary by a factor of two over a solar cycle (Pap, London and Rottman 1991), and from 5% to 40% over one solar rotation (Lean and Skumanich 1983). The quiet Sun Lyα profile is marked by a central self-reversal that dips to about 60% of the peak intensity, and by steep non-gaussian wings (Lemaire *et al.* 1978). Spatially resolved observations show considerable variation in both the amount of self-reversal, and ocassionally in the asymmetry and the shape of the line wings. The line self-reversal is usually, but not always, less prominent in solar active regions. The chromospheric network shows up clearly in high-resolution Lyα filtergrams of the Sun (Bonnet *et al.* 1980), while solar active regions tend to show a loop structure more characteristic of transition-region plasma. The recent solar transition regions models of Fontenla, Avrett, & Loeser (1991), which include the effects of ambipolar diffusion, place the formation of the Lyα core at 40,000 K, with the wings formed throughout the chromosphere down to the temperature minimum.

Most high-dispersion stellar Lyα studies have concentrated on deriving properties of interstellar H I and D I along the line of sight (e.g., Murthy *et al.* 1987). The main re-

sult concerning the intrinsic stellar Lyα emission has been the Wilson-Bappu or linewidth-luminosity relation for Lyα, which we discuss in the next section, but some other results from high-dispersion studies can be noted. Linsky *et al.* (1992) obtained high spectral resolution ($\lambda/\Delta\lambda = 84,000$), high signal/noise GHRS spectra of the Lyα profile of Capella (G0 III + G8 III). They found the Lyα wings of the dominant G0 star to be considerably shallower than the wings of the solar profile, and that a red asymmetry must exist in the intrinsic profile of either or both of the G star components. The only other star for which an intrinsic asymmetry is required to explain the observed Lyα profile is α Boo (McClintock *et al.* 1975). Woodgate *et al.* (1992) detected a rapid (3s) brightening in the red wing of the GHRS Lyα profile of the dMe star AU Mic, which they attribute to the effects of a proton beam during the impulsive phase of a flare. Neff *et al.* (1990) obtained IUE high-dispersion Lyα profiles of high-radial velocity stars, where the center of the Lyα emission is Doppler shifted away from the interstellar core. The observed profiles must still be corrected for absorption by the damping wings of the interstellar H I absorption, but the red wing of the intrinsic self-reversal does appear to be detected in the profile of the metal-poor G8 III giant δ Lep.

4.2 Synthetic Lyα profiles

Figure 2 shows how the solar Lyα profile would appear if it were placed behind various H I column densities. For this calculation we have adopted the solar profile of Lemaire *et al.* (1978), which we parameterize with a gaussian self-reversal and piece-wise linear fit to the wings. We set the FWHM to 0.72 Å and the depth of the self-reversal to 80% of the peak intensity. The attenuated profiles are computed by multiplying this solar profile by the appropriate interstellar Voigt H I and D I profiles. In our nominal interstellar model, we assume a deuterium number abundance of 1.5×10^{-5}, a value supported by two recent studies (McCullough 1992, Linsky *et al.* 1992). Various temperature determination of the local interstellar gas are in the range 7000 - 12000 K (Frisch *et al.* 1990). We have selected a value of 7300 K (corresponding to a H I velocity dispersion of 11 km s^{-1}), based on the analysis of the interstellar profile observed toward Capella with GHRS by Linsky *et al.* (1992)

We then integrated the attenuated profiles over wavelength to derive the amount by which the intrinsic stellar flux is attenuated by interstellar absorption. Figure 3 illustrates the dependence of the Lyα attenuation upon adopted stellar and interstellar parameters. An increase in the interstellar H I velocity dispersion in our models to 14 km s^{-1} reduces saturation effects in the absorption profile and increases the total attenuation. A similar effect should occur if the interstellar gas is characterized by multiple velocity components, as has been seen in certain directions in the LISM (Lallement, Vidal-Madjar, and Ferlet 1986).

The interstellar attenuation is reduced when the intrinsic stellar profile is given a deeper self-reversal, down to 0.4 of the peak intensity, or if we impose a velocity shift of 20 km s^{-1} between the centroid of the stellar emission and the local interstellar medium. (Note that the Lyα flux from a spectroscopic binary might show variations simply due to a periodic velocity shift with respect to the flow velocity of the LISM.) Given the close agreement of the curves drawn in Figure 3, we can say that none of these effects introduce a large uncertainty in estimating the total interstellar attenuation.

On the other hand, the total amount of interstellar attenuation *does* critically depend on the linewidth of the stellar emission, because the interstellar core absorbs proportionally less of a broad line than of a narrow line. This dependence of the attenuation at Lyα on the FWHM of the stellar emission line is illustrated in Figure 4. An H I column density of 5×10^{18} cm^{-2}, for example, attenuates the flux from a FWHM = 0.72 Å profile by a factor of ten, but that of a FWHM = 2.1 Å profile by only a factor of two. As an aid to the reader, Figure 5 provides a contour plot which allows the Lyα attenuation factor to be quickly estimated if the FWHM of the stellar emission line and the intervening interstellar H I column density are both known.

These calculations demonstrate that one has to estimate the linewidth of the stellar Lyα emission before one can estimate the interstellar attenuation. Fortunately, the Lyα line appears to obey a linewidth-luminosity relationship analogous to the Wilson-Bappu relations for Mg II and Ca II. A qualitative illustration of this effect in Lyα is shown in Figure 6, which displays high-dispersion Lyα profiles of five stars of absolute magnitude ranging from 6.1 to -0.5. The quantitative determination of the stellar Lyα linewidth is not straightforward because the peak intensity of the line is not directly observed. The interstellar core of the line must be modeled, and the observed profile mulitplied by e^{τ} to reconstruct the intrinsic stellar profile. The linewidth can then be measured on the reconstructed profile, after correcting for instrumental broadening. Neff *et al.* (1986) applied this technique to IUE high-dispersion profiles of ten stars to derive the following relationship

$$M_V = (33.2 \pm 3.7) - (12.4 \pm 1.5) \log W_0 \qquad (1)$$

where M_V is the absolute visual magnitude and W_0 is the Lyα width line in km/s.

The least luminous star studied by Neff *et al.* was ϵ Eri at $M_V = 6.1$. Ambruster, Pettersen, and Sundland (1989) present evidence that the Mg II Wilson-Bappu relation is linear over a total range of 17 mag in M_V , down to the faintest star studied (AT Mic) at $M_V = 11.4$. Whether the Lyα Wilson-Bappu relation can be extrapolated to such faint magnitudes is less certain. The linewidths of both ϵ Eri and α Cen B ($M_V = 5.7$) are somewhat broader than predicted by the mean relation of Neff *et al.*, while high dispersion

Lyα profiles of AU Mic (M_V = 8.6) obtained with IUE (Ayres *et al.* 1983) and with GHRS (Woodgate *et al.* 1992) appear to be at least as broad as the solar Lyα profile. A similarly broad Lyα profile is seen in the high-dispersion IUE spectrum (SWP 26672) of AT Mic. The IUE and GHRS profiles of these dMe stars are from large aperture observations which are contaminated by geocoronal Lyα, and so that it is not possible to reconstruct from these data the intrinsic stellar profile, for the purpose of extracting the Lyα linewidth. In the absence of any better option, we have, therefore, assumed a linewidth of 0.7 Å (173 km s^{-1}) for all stars with $M_V > 5.5$. When small-aperture GHRS Lyα profiles of the dMe stars become available, then a better determination of the linewidth can be made. Until then, however, the intrinsic Lyα flux of these stars should be considered extremely uncertain.

To compute a synthetic stellar Lyα profile of a given linewidth, we have applied a simple linear rescaling in wavelength to the solar Lyα profile. Real stellar profiles may be poorly represented by such a simple rescaling of the solar profile. Linsky *et al.* (1992) suggested that a power-law rescaling of the wavelength variable of the solar profile could better match the shallow Lyα wings of the Capella giants. The errors introduced by adopting an incorrect profile will increase at large column densities, when most of the observed flux arises from the far wings of the Lyα emission. Figure 3 illustrates this effect by comparing the attenuation of a solar-like profile with that of a gaussian profile of the same FWHM. The discrepancy in the attenuation factor between the two adopted profiles increases with N(H I), up to a factor of two discrepancy at 5×10^{18} cm^{-2}. Because of this uncertainty in the behavior of the Lyα wings, we attempt to recover the intrinsic Lyα flux only of stars in low column density directions of the LISM.

4.3 A Model of the LISM

Studies of the LISM show a striking anisotropy in the distribution of H I gas. For example, the H I column density estimated toward Altair (log N(H I) = 18.7 - 19.1; deBoer *et al.* 1986), at a distance of 5 pc, is larger than the column density determined toward β CMa (log $N(H\ I) = 18.0 - 18.3$; Gry, York, & Vidal-Madjar 1985), at a distance of 200 pc. In the low-density directions, the LISM appears to be devoid of H I beyond 2-3 pc from the Sun, with a total column density within a factor of two of 1.5×10^{18} cm^{-2}. Enhancements in the soft X-ray background in these directions suggest that the H I cavity is filled with a hot ($T \sim 10^{6.0}$ K) plasma (Snowden *et al.* 1990).

In Table 2 we estimate the intrinsic Lyα flux of those stars which are either located in the low-density region of the LISM, or which have interstellar H I column densities available in the literature. We define the low-density region of the LISM to include those stars with

distance (d, in pc) and galactic longitudes and latitudes (l,b) satisfying any of the following conditions: (1) $b > 50$, (2) $120 < l < 290$ and $d < 50$, or (3) $d < 5$. The selected stars fall roughly within the low-density region outlined by Génova *et al.* (1990) on the basis of interstellar Mg II observations of 51 stars within 30 pc of the Sun. They also avoid all eight nearby interstellar clouds within 100 pc listed by Frisch & York (1991), plus the nearby clouds found by Lilienthal and de Boer (1991) and Centurion & Vladilo (1991), as well as the directions found to have a multi-component ISM structure by Lallement, Vidal-Madjar, & Ferlet (1986).

The intrinsic Lyα flux for the 149 selected stars is computed as follows. First, the stellar absolute magnitude M_V is determined from either the stellar parallax, when known, or from spectral type information. This value of M_V is then used to compute an expected emission FWHM from the Lyα Wilson-Bappu relation discussed in §4.2. An emission profile is created by linearly rescaling a solar-type profile to this FWHM. The emission profile is multiplied by an ISM aborption profile with either a direct column density estimate from the literature or N(H I) = 1.5×10^{18} cm^{-2}. The shift between the centroid of the stellar emission and the interstellar H I absorption is computed using the stellar radial velocity, and the velocity vector of the LISM given in Frisch & York (1991). The depth of the self-reversal and remaining ISM parameters are set in accordance with the nominal model of §4.2.

The factors needed to recover the intrinsic Lyα flux for the stars listed in Table 2 range from ~ 1.4 for the nearby giants to ~ 5.3 for the dM stars. The uncertainty in the attenuation factor is probably about 20% for the giants ranging up to a factor of two for the dM stars. These uncertainties are estimated by assuming a 10% uncertainty in the stellar FWHM and a 50% uncertainty in the interstellar H I column density. When more than one Lyα flux measurement of a star is given in Table 1, we selected the highest quality measurement to derive the intrinsic Lyα flux in Table 2. The quality indicies given in Table 2 are derived by combining in quadrature the estimated measurement error and the uncertainty in the attenuation factor. An empirical determination of the uncertainty can be estimated using flux-flux plots, to be discussed in §5.1, which correlate the Lyα flux against other measures of stellar activity. The scatter in these relations can be used to provide an upper limit to the uncertainties in computing the interstellar attenuation factor, subject to the condition that the Sun should not occupy an anomalous position in the diagrams.

The H I gas which attenuates the stellar Lyα emission is also mainly responsible for absorption at wavelengths < 912 Å. Many of the stars in our Lyα catalog are likely to be also detected as EUV sources (Vedder *et al.* 1991), and it is of interest to compare the computed attenuation at Lyα with that expected in the EUV. Figure 4 compares the attenuation

factor expected for stellar Lyα, with that expected at 300 Å, 400 Å, and 550 Å. To compute the EUV attenuation at wavelengths less than 504 Å, we have assumed a neutral helium abundance of N(H I)/N(He I) = 12 (Kimble *et al.* 1992). The EUV extinction has a steeper dependence on N(H I) because of saturation effects in the interstellar Lyα absorption line. Nevertheless, Figure 4 shows that measurements of both Lyα emission and EUV emission toward the same star can provide valuable constraints on the H I column density along the line of sight.

5 Discussion

This paper gives a catalog of "observed" Lyα fluxes for 275 stars in Table 1, and a catalog of approximate "intrinsic" Lyα fluxes in Table 2 for 149 stars for which an interstellar attenuation factor could be estimated. The intrinsic flux catalog should be used to obtain quantitative estimates of the radiative losses in Lyα, to study Lyα excitation of fluorescent lines, and to derive flux-flux relations between Lyα and other measures of stellar activity. However, there do exist some applications that require no knowledge of the model-dependent interstellar attenuation factor, and for these uses the "observed" catalog will suffice.

The simplest use of the observed flux catalog is to provide a firm lower limit on the intrinsic Lyα flux. The utility of this lower limit is demonstrated by the fact that more than half the stars in the catalog have a normalized Lyα flux that is larger than the Sun's. The mere presence of Lyα emission can also be a useful diagnostic in the late A-type stars where other, more common chromosphere diagnostics can fail because of a poor contrast with the photospheric continuum. The observed Lyα flux can also be used to monitor chromospheric variability (e.g., Vilhu, Neff and Rahunen 1989) since, for a given star, the interstellar attenuation factor remains constant. Finally, the observed flux catalog is useful for computing exposure times and selecting targets for future high dispersion Lyα observations.

5.1 Stellar Activity in the HR diagram

Figure 7 shows the observed normalized Lyα flux, R(Lyα) plotted as a function of B–V, while Figure 8 shows the same relation for the intrinsic Lyα fluxes. The general appearance of the two figures is similar, although the absolute flux levels in Figure 8 are 2-5 times larger due to the correction for interstellar absorption. In particular, Figure 8 shows that all main sequence stars have a normalized Lyα flux larger than that of the full-disk solar Lyα emission at solar minimum. The very weakest fluxes are associated with the coolest giant stars, which show only weak traces of chromspheric emission in all other UV lines accessible to IUE

(Linsky & Haisch 1979) and no coronal X-ray flux to extremely low detection levels (Ayres, Fleming, & Schmitt 1991). In nearly all stars the radiation losses in Lyα are comparable to those in Mg II.

The top panels of Figure 7 and Figure 8 show that the spread in Lyα flux at a given color index is roughly a factor of 10 (1 dex) at $0.3 < B-V < 0.6$ but a factor of 100 (2 dex) at $B-V > 0.6$ (i.e., among the late G-M stars). The brightest fluxes among the coolest stars belong to the spotted stars of the BY Dra class and of the RS CVn category. Both types of stars are extremely rare at earlier spectral types, which accounts for the narrower range in emission that we have found. Among the stars of solar-type, the spread in Lyα emission is linked to the rotation speed, and hence statistically to the age, of the star, as has been found previously for other chromospheric and coronal emissions (Simon *et al.* 1985).

A total of 14 stars with $B-V \leq 0.29$ were detected at Lyα. However, the emission level of the detected stars is generally lower than that found for cooler stars, and numerous stars with $B-V \leq 0.29$ are *not* detected at Lyα. This behavior is similar what we have previously reported for C II emission (Simon and Landsman 1991). The agreement is important because the observational selection effects are quite different for the two lines. The detection of C II in these hotter stars is limited by blending with the photospheric absorption features, while at Lyα, where the contrast with the continuum is much larger, the detection is limited chiefly by the effects of gecoronal contamination and interstellar absorption.

5.2 Correlations with C II and X-ray emission

Flux-flux plots of many of the chromospheric and transition lines observed in IUE spectra show tight power-law relationships independent of spectral type or of binarity (Ayres, Marstad, and Linsky 1981, Oranje 1986). A flux-flux relationship between Lyα and a different emission line, unaffected by interstellar absorption, would be a powerful diagnostic for estimating interstellar H I column densities. In the Sun, variations in the solar Lyα flux are known to correlate well with variations in C II and C IV both in the temporal variation of full disk fluxes (Mount & Rottman 1985), and in the spatial variations of different regions across its surface (Schrijver *et al.* 1985).

The most useful spectral line to compare with Lyα may be C II 1335 Å which is thought to be formed in the high chromosphere at temperatures near 15,000 K. The C II doublet is uncontaminated by blending with other lines at the IUE low-dispersion resolution (Capelli *et al.* 1989), and the proximity of C II in wavelength to Lyα means that it has a similar high contrast with the photospheric continuum in the F- and later type stars. The C II

flux can often be measured on the same IUE image as the Lyα flux, so that any effects of chromospheric variability are minimized. Figure 9 shows the ratio of f(Lyα) / f(C II) for stars with good measurements in both lines, where the observed Lyα flux has been used uncorrected for interstellar absorption. A few of the C II measurements are new, but most have taken from the literature (Simon and Landsman 1991; Simon and Drake 1989; Simon and Fekel 1987). The singular position of the Sun in this figure highlights the presence of interstellar attenuation of the Lyα fluxes. This was not as evident in the plot of normalized fluxes, Figure 8, because the attenuation of the stellar Lyα fluxes is partially compensated by the fact that most of the catalog stars are more chromospherically active than the Sun. The position of the Sun does not appear anomalous when intrinsic Lyα fluxes are used (Figure 10) which provides evidence that our correction scheme for interstellar absorption is approximately right.

In Figure 10, the ratio of f(Lyα)/f(C II) appears to increase with B–V up until B–V = 0.6 where it approximately levels off. This trend with B–V could, in principle, be due to an improper correction for interstellar absorption, because the correction tends to be smaller for the earlier type stars, which are on average more luminous, and are thus predicted to have broader Lyα lines. However, the larger line widths predicted for the A-F stars are confirmed for Procyon, β Cas, and α Aql, where high dispersion spectra are available. In addition, the same trend with color appears, although not as strong, in the plot of uncorrected Lyα fluxes (Figure 9), and so cannot be entirely an artifact of the adjustments we have made for interstellar absorption.

Because of the dependence of f(Lyα)/f(C II) on B–V color, there is no correlation between the strength of these two lines among stars with B–V < 0.6. However, Figure 11 shows that a good nearly, linear correlation exists for stars with B–V > 0.6. This is in agreement with the results of Schrijver *et al.* (1985) who found a linear correlation between Lyα and C II in selected solar regions.

The rapidly rotating G giant ψ^3 Psc (G0 III, $v \sin i$= 95 km s^{-1}), is conspicuous in Figure 11 by its low flux in Lyα. Both this star, at f(Lyα)/f(C II) = 1.9, and 35 Cnc (G0 III,$v \sin i$= 87 km s^{-1}) at f(Lyα)/f(C II) < 2.8, are conspicuous in Figure 9 by their very low flux ratios. Although the interstellar column density toward 35 Cnc ($l = 206$, $b = 31$, d $\sim$ 120 pc) is uncertain, ψ^3 Psc (l = 129, b = -43, d $\sim$ 75 pc) is located in the low density region of the LISM and so heavy interstellar attenuation is unlikely to account for the anomalous position of this star. An intruiging possibility is that the weakness of Lyα, for ψ^3 Psc at least, is related to the enormous X-ray deficit (relative to transition region line fluxes) found for this star by Simon and Drake (1989). It is interesting, although perhaps only coincidental,

that the R(Lyα) value in ψ^3 Psc is comparable to the flux observed for much more evolved, slowly rotating red giants located to the right of the Hertzprung gap.

The low values of f(Lyα)/f(C II) exhibited by the F stars in our sample, as well as by the pair of rapidly rotating G giants, coupled with the X-ray deficit reported for these stars (Simon & Drake 1989), suggested to us that Lyα may correlate better with the X-ray flux than with C II. The number of stars with X-ray measurements is currently not as large as the number with C II data, but we were able to find published X-ray fluxes for 58 stars from Table 2, i.e., for stars that also have intrinsic Lyα flux determinations. As demonstrated by Figure 12, Lyα correlates very well with X-ray emission. From this log-log plot we derive a power-law relation with an exponent of 1.52 ($\pm$0.11). For comparison, Schrijver *et al.* (1985) found a power-law exponent of 1.40 when comparing the Lyα and X-ray flux of 12 different solar regions (although we could not confirm this relation using their tabulated fluxes). Exceptions to the Lyα – X-ray correlation exist only for the A stars (α Aql and α Cep), and for the cool giants, consistent with a lack of high temperature material in both groups of stars.

Additional evidence that the coronal X-ray flux correlates better with Lyα than it does with C II is provided by the detailed study of the GHRS Lyα profile of Capella binary by Linsky *et al.* (1992). These authors estimated that the Lyα luminosity of the G0 star is about 1.6 times the luminosity of the G8 star. Ayres, Schiffer, & Linsky (1983) estimated that the soft X-ray luminosities of the two components were approximately equal. In contrast, Ayres (1988b) found a flux ratio about 3 for low excitation lines like Mg II, and about 10 for the transition region lines of C II and C IV.

Finally, the correlations found between the Lyα and C II, or between Lyα and X-ray emission, can be used, in principle, to derive approximate H I column densities in the LISM. The C II or X-ray emission can be used to predict the intrinsic stellar Lyα flux, and the interstellar attenuation factor determined by comparison with the observed Lyα emission. We defer a complete discussion of this method to a subsequent paper, but give here an example that also justifies the some of the assumptions used in Section 4.3. Figure 13 shows a Lyα – C II flux–flux plot for those stars in the "high-density" region of the LISM, i.e., the stars for which we did not estimate an H I column density in Section 4.3. In this example, we assumed that N(H I) = 1.5×10^{18} cm^{-2}, the same column density assumed for stars in the low-density region. Figure 13 shows that this is a bad assumption for the stars in the high-density region, and that larger interstellar column densities must exist toward these stars if they are to satisfy the flux-flux relation determined in Figure 11.

6 Future Work

There are several areas of future observational work which would contribute to the study of Lyα emission in late-type stars. Many of the brightest Lyα sources in the sky, such as HR 1099 and α Tau, have poorly determined absolute Lyα fluxes because all existing IUE low-dispersion images of these stars are saturated at Lyα. Additional IUE low-dispersion observations with exposure times optimized for the Lyα feature would provide more accurate fluxes for these stars. Additional high-dispersion Lyα observations with GHRS or IUE would better constrain the Lyα Wilson-Bappu relation and test its range of validity. A more detailed H I column density map of the LISM, and thus more accurate estimates of the interstellar Lyα attenuation, should be possible using absorption line studies with GHRS and from EUV studies with the recently launched EUVE satellite. Finally, the many more X-ray observations that will ultimately be provided by the ROSAT All Sky Survey will lead to a much better test of the correlation between Lyα and X ray fluxes presented in this work.

This research was supported in part by NASA grant NAS 5-30446 to Hughes/STX, and by NASA grants NAG 5-146 and 5-1823 to the University of Hawaii.

REFERENCES

Ahmad, I. A., 1986, DIPS Conversion Documentation (Bethesda, MD: Imad-ad-Dean, Inc.) IAD 86-1A

Ambruster, C.W., Pettersen, B.R., & Sundland, S.R., 1989, A&A, 208, 198

Ayres, T. 1988a, IUE Newsletter No. 35, 137

Ayres, T. 1988b, ApJ, 331, 467

Ayres, T.R., Eriksson, K., Linsky, J., & Stencel, R.E. 1983, ApJ, 270, L17

Ayres, T.R., Fleming, T.A., & Schmitt, J.H.M.M. 1991, ApJ, L45

Ayres, T.R., Marstad, N.C., & Linsky, J.L. 1981, ApJ, 247, 545

Ayres, T.R., Schiffer, F.H., & Linsky, J.L. 1983, ApJ, 272, 223

Basri, G.S., Linsky, J.L., Bartoe, J.-D.F., Brueckner, G., & Hoosier, M.E.V, 1979, ApJ, 230, 924

Blondel, P.F.C., Talavera, A. & Tjin A Djie, H.R.E. 1992, A&A, in press

Bohlin, R.C. & Grillmair, C.J. 1988, ApJS, 68, 487

Bohlin, R.C., Harris, A.W., Holm, A.V., & Gry, C. 1990, ApJS, 73, 413

Bohlin, R.C., Holm, A.V., Savage, B.D., Snijders, M.A.J., & Sparks, W.M. 1980, A&A, 85, 1

Böhm-Vitense, E. & Woods, J. 1983, ApJ, 265, 331

Bonnet, R.M., Bruner, E.C., Acton, L.W., Brown, W.A., & Decaudin, M. 1980 ApJ, 237, L47.

Bruhweiler, F.C., & Vidal-Madjar, A. 1987, in Exploring the Universe with the IUE Satellite, ed. Y. Kondo, (Dordrecht: Reidel), 467

Byrne, P.B., & Doyle, J.G. 1989, A&A, 208, 159

Byrne, P.B., & Doyle, J.G. 1990, A&A, 238, 221

Cappelli, A., Cerruti-Sola, M., Cheng, C.C., & Pallavicini 1989, A&A, 213, 226

Cassatella A., Barbero, J. & Benvenuti, P. 1985 A&A, 144, 335

Cassatella A., Ponz, D., & Selvelli, P.L. 1983, IUE Newsletter No. 21, 46

Catalano, S., Bruno, M. & Marilli, E. 1986, Advances in Space Research, 6, No. 8, 207

Catalano, S., Marilli, F., Freire Ferrero, R., & Gouttebroze, P. 1991, A&A, 250, 573

Centurion, M., & Vladilo, G. 1991, ApJ, 372, 494

Clarke, J., Bowyer, S., Fahr, H.J., & Lay, G., 1984 A&A, 139, 389

Clarke, J. *et al.* 1986, J. Geophys. Res., 91, 8771

deBoer, K.S., Lenhart, H., van der Hucht, K.A., Kamperman, T.M., Kondo, Y., and Bruhweiler, F.C. 1986, A&A, 157, 119

Doyle, J.G., Panagi, P., & Byrne, P.B. 1990, A&A, 228, 443

Fontenla, J., Reichmann, E.J., & Tandberg-Hanssen, E. 1988, ApJ, 329, 464

Fontenla, J.M., Avrett, E.H., & Loeser, R. 1991, ApJ, 377, 712

Fricke, K. H., & Ojanguren, O. 1980, in Proc. 2d European IUE Conf., ed. B Battrick & J. Mort (ESA SP-157), 3

Frisch, P.C., Welty, D.E., York, D.G., & Fowler, J.R. 1990, ApJ, 357, 514

Frisch, P.C., & York, D.G. 1991, in Extreme Ultraviolet Astronomy, ed. R. Malina, & S. Bowyer, (New York, Permagon Press), 322

Génova, R., Molaro, P., Vladilo, G. & Beckman, J.E. 1990, ApJ, 355, 150

Gliese, W., & Jahreiss, H. 1991, Catalogue of Nearby Stars, prelim. 3rd edition, Astronomical Data Center CDROM (NASA, National Space Science Data Center)

Gry, C., York, D.G., Vidal-Madjar, A. 1985, ApJ, 296, 593

Hallam, K.L., Altner, B., & Endal, A.S. 1991, ApJ, 372, 610

Hoffleit, D. & Warren, W.H. Jr. 1991, The Bright Star Catalogue, prelim. 5th edition, Astronomical Data Center CDROM (NASA, National Space Science Data Center)

Imhoff, C.L. 1986, IUE Newsletter No. 31, 11

Kimble, R.A. *et al.*, 1992, ApJ, in press

Lallement, R., Vidal-Madjar, A., & Ferlet, R. 1986, A&A, 168, 225

Landsman, W., & Simon, T. 1991, ApJ, 366, L79

Landsman, W.B., Henry, R.C., Moos, H.W., & Linsky, J.L., & Russell, J.L. 1984, ApJ, 285, 801

Landsman, W.B., Murthy, J., Henry, R.C., Moos, H.W., Linsky, J.L. & Russell, J.L. 1986, ApJ, 303, 791

Lean, J.L. & Skumanich A., 1983, J. Geophys. Res. 88, 5751

Lemaire, P. Charra, J., Jouchoux, A., Vidal-Madjar, A., Artzner, G.E., Vial, J.C., Bonnet, R.M., & Skumanich, A. 1978, ApJ, 223, L55

Lilienthal D. & de Boer, K.S. 1991 A&AS, 87, 471

Linsky, J.L., Brown, A., Gayley, K., Diplas, A., Savage, B.D., Landsman, W., Shore, S.N., & Heap, S.R.. 1992, ApJ, in press

Linsky, J.L, & Haisch, B.M. 1979, ApJ, L27

McClintock, W., Linsky, J.L., Henry, R.C., Moos, H.W., & Gerola, H. 1975, ApJ, 202, 165.

McCullough, P.R. 1992, ApJ, 390, 213

Mount, G.H. & Rottman, G.J. 1985, J. Geophys. Res., 90, 13031

Muñoz-Peiro, J.R. 1986, IUE Newsletter No. 27, 27

Murthy, J., Henry, R.C., Moos, H.W., Landsman, W.B., Linsky, J.L., Vidal-Madjar, A., & Gry, C. 1987, ApJ, 315, 675

Neff, J.E., Landsman, W.B., Bookbinder, J.A., & Linsky, J.L. 1990, in Evolution in Astrophysics, (ESA SP-310), 341

Neff, J.E., Linsky, J.L., Landsman, W.B., & Carpenter, K.G., 1986, in New Insights in Astrophysics, (ESA SP-263), 669

Oranje, B.J. 1986, A&A, 154, 185

Pap, J.M., London, J., & Rottman, G.J. 1991, A&A, 245, 648

Rottman, G.J. 1981, J. Geophys. Res., 86, 6697

Rucinski, S.M., Vilhu, O., Whelan, J.A. 1985, A&A, 143, 153

Schrijver, C.J., Zwaan, C., Maxson, C.W. & Noyes, R.W. 1985, A&A, 149, 123

Simon, T., & Drake, S.A., 1989, ApJ, 346, 303

Simon, T., & Fekel, F.C. 1987, ApJ, 316, 434

Simon, T., Herbig, G., and Boesgaard, A.M. 1985, ApJ, 293, 551

Simon, T., & Landsman, W.B., 1991, ApJ, 380, 280

Snowden, S.L., Cox, D.P., McCammon, D., & Sanders, W.T. 1990, ApJ, 354, 211

Strassmeier, K.G., Hall, D.S., Zelik, M., Nelson, E., Eker, Z. & Fekel, F.C. 1988, A&AS, 72, 291

Thompson, R. 1988, IUE Newsletter No. 35, 108

Vedder, P.W., Vallerga, J.V., Jelinsky, P., Marshall, H.L., & Bowyer, S. 1991, in Extreme Ultraviolet Astronomy, ed. R. Malina, & S. Bowyer, (New York, Permagon Press), 120

Vilhu, O., Neff, J.E. & Rahunen, T. 1989, A&A, 208, 201

Woodgate, B.E., Robinson, R.D., Carpenter, K.G., Maran, S.P., & Shore, S.N. 1992, ApJ, 397, L95

This manuscript was prepared with the AAS WGAS LaTeX macros v2.2

Figure Captions:

Figure 1: Our method of removing diffuse Lyα emission is illustrated for the 70 minute IUE observation SWP 28544 of the F0IV star, HR 2740. Figure 1a shows the original line-by-line image. The large aperture is illuminated by diffuse Lyα, while the (scattered light) continuum of HR 2740 is concentrated toward the center of the aperture. Figure 1b shows the same region after a sky-only image has been scaled to match the edges of the aperture, and then subtracted off. Figures 1c and 1d show the resulting 1-D spectrum before and after subtraction of the diffuse component.

Figure 2: A model solar Lyα profile is shown as it would appear if observed through H I column densities of 0, 0.5, 1, 2, and 5 $\times 10^{18}$ cm^{-2}.

Figure 3: The solid line shows that amount a solar-type Lyα profile would be attenuated as a function of N(H I), using the nominal parameters described in the text. The remaining lines show the influence of changing a single parameter in the nominal model. The dotted line shows attenuation expected when a velocity shift of 20 km s^{-1}is imposed between the stellar and interstellar centroids. The short dashed line shows the effect of increasing the interstellar velocity dispersion to 14 km s^{-1}. The dot-dash line shows the change caused by increasing the strength of the intrinsic self-reversal, to 40% of the peak intensity. The long dashed line shows the effect of representing the stellar emission by a gaussian profile of the same FWHM as the solar-type profile

Figure 4: The solid lines show the attenuation factor of the integrated Lyα flux of a stellar emission profile as a function of N(HI), for an assumed emission FWHM of 0.72 Å, 1.5 Å, and 2.1 Å. The dotted lines denote the EUV attenuation as a function of N(H I) at 300 Å, 400 Å, and 550 Å.

Figure 5: A contour plot showing the lines of constant attenuation factor computed for synthetic Lyα profiles having the nominal stellar and interstellar parameters discussed in the text. This plot allows the interstellar Lyα attenuation factor to be estimated if the interstellar column density and the stellar emission FWHM are known.

Figure 6: IUE Lyα high dispersion profiles are shown for five stars of various absolute magnitudes. The profiles of α Cen A and α Cen B are taken from Landsman *et al.* (1986) and are co-additions of several IUE images. The profile of α CMi is taken from the IUE small aperture image SWP 26917. The profiles of β Cet and γ Cru are taken, respectively, from the IUE large-aperture images, SWP 14786 and SWP 44137, with diffuse Lyα emission removed as explained in the text.

Figure 7: The observed normalized Lyα fluxes from Table 1, are shown as a function of B–V, (a) for B–V < 0.50 and (b) for B–V > 0.50. Stars of luminosity class V or IV-V are plotted as inverted triangles, those of class IV as triangles, and the more luminous stars as circles. Open symbols represent more uncertain measurements. Note much larger range of normalized Lyα fluxes found in (b) for the cooler stars. The solid error bar at B–V = 0.66 shows the range of full-disk normalized Lyα fluxes observed over a solar cycle according to Lean and Skumanich (1983). The dotted line error bar at B–V = 0.66 shows the range of Lyα intensities observed in individual solar features (e.g., dark points and plages) reported by Basri *et al.* (1979).

Figure 8: Same as Figure 7 except that the intrinsic (i.e. corrected for interstellar absorption) Lyα fluxes from Table 2 are displayed.

Figure 9: The observed Lyα/C II flux ratio is shown as a function of B-V. The meaning of the symbols is the same as in Figure 7. The range of this ratio in the Sun (20 < f(Lyα)/f(C II) < 38) is also indicated at B–V = 0.66, and is taken from the full disk measurements of Rottman (1981) and Mount and Rottman (1985) for solar minimum and maximum.

Figure 10: Same as Figure 9 except that the Lyα flux values have been corrected for interstellar absorption. The low value at B–V = 0.68 is the star ψ^3 Psc.

Figure 11: The normalized intrinsic Lyα flux is plotted against the normalized C II flux for the stars with B–V > 0.6. The meaning of the symbols is the same as in Figure 7. The dotted line shows the best-fit relation log R(Lyα) = 1.81 + 0.99($\pm$0.04) $\times$ log R(C II). The regression excluded the upper and lower limits, the giants with B–V > 1.0, and the star ψ^3 Psc.

Figure 12: The normalized X-ray flux is plotted against the normalized Lyα flux. The meaning of the symbols is the same as in Figure 7. The dotted line shows the best-fit relation log R(Xray) = 1.79 + 1.52($\pm$0.11) $\times$ log R(Lyα). The figure and the regression exclude the stars with B–V < 0.30 and the giants with B–V > 1.0.

Figure 13: The normalized Lyα flux of the stars with B–V > 0.6 in the "high-density" region of the LISM is plotted against their normalized C II flux. The meaning of the symbols is the same as in Figure 7. The Lyα fluxes have been corrected for an interstellar attenuation of 1.5×10^{18} cm^{-2}, which is the same column density assumed in this paper for the stars in the "low-density" region. The dotted line shows the best-fit regression determined in Figure 11 for the stars in the low-density region of the LISM. The Lyα fluxes of the star in the high-density region deviate systematically below the regression line, confirming our assumption that the Lyα attenuation toward these stars is indeed larger.

Table 1
Lyman Alpha Fluxes

Star	HD	Spectral Type	V	$B-V$	Image	Exposure (s)	f(Lyα) (10^{-14})	R(Lyα) (10^{-7})
δ^3 Tau	27819	A7 V	4.80	0.15	4446	1020	<140	<50
80 UMa	116842	A5 V	4.01	0.16	15180	1080	<250	<42
ι UMa	76644	A7 IV	3.14	0.19	31955	120	<1540	<120
γ Boo	127762	A7 III	3.03	0.19	2395	1440	<250	<17
					3427[a]	6000	1500:	12
					23043[a]	15000	1900::	16
α Aql	187642	A7 V	0.77	0.22	28546	180	<4000	<33
					29566	180	<6940	<58
					33604	120	2400:	20
α Cep	203280	A7 V	2.44	0.22	28560	450	110:	4.2
θ Tuc	3112	A7 IV	6.13	0.23	31882	9000	83::	98
22 Boo	126661	F0m	5.39	0.23	31248	1200	<87	<52
38 Ari	17093	A7 V	5.18	0.24	42318	1800	<77	<38
45 Ori	37077	F0 III	5.26	0.24	42312	2700	<100	<55
49 UMa	95310	F0 V s	5.08	0.24	4009	1500	<85	<38
ϵ^1 Nor	143474	A7 IV	4.63	0.24	42310	1200	<66	<20
9 Lac	214454	A8 IV	4.63	0.24	42765	2100	<43	<13
ω Aqr	222345	F0 IV	5.00	0.24	42766	2880	<98	<41
κ^2 Tau	27946	A7 V	5.28	0.25	42298	3600	44::	24
					42764	4500	<27	<14
71 Tau	28052	F0 V	4.49	0.25	9874	1200	98:	25
					32102	720	200::	50
					32140	2100	83:	21
HR 1507	30034	F0 V	5.40	0.25	42299	4200	43::	26
HR 3350	71935	A9-F0 III-IV	5.09	0.25	31883	4320	<55	<24
HR 4017	88824	A7 V	5.28	0.25	28543	8400	<38	<20
HR 4086	90132	A8 V	5.33	0.25	30296	4680	<46	<26
30 LMi	90277	F0 V	4.74	0.25	32151	1020	59::	19
υ Tau	28024	A8 Vn	4.28	0.26	2672	1200	<140	<30
83 Tau	28556	F0 V	5.40	0.26	32101	1200	<180	<110
HR 1480	29499	A5m	5.39	0.26	27890	3600	<52	<31
64 Eri	32045	F0 IV	4.79	0.26	42300	2400	<64	<22
ν^1 Dra	159541	A6 V	4.88	0.26	1408	600	<61	<22
ξ Ser	150876	F0 IV	3.54	0.26	6181	119	<210	<23
					6182	599	<200	<21
28 Aql	181333	F0 III	5.53	0.26	31957	1080	<130	<85
η Hor	16555	A6 V	5.31	0.27	29564	6000	<37	<20
15 UMa	78209	F0 IVm vs	4.48	0.27	31956	360	<490	<120
					32103	840	<73	<19
14 Com	108283	F0p	4.95	0.27	33608	1380	<43	<17
σ Oct	177482	F0 III	5.47	0.27	42767	2400	<52	<33
η Ind	197157	A7 III-IV-A9	4.51	0.27	28548	3420	<50	<13
α Hyi	12311	F0 V	2.86	0.28	1621	60	<170	<10
					32139	600	150::	8.4
					33605	900	120:	7.0
51 Tau	27176	F0 V	5.05	0.28	32184	1500	<110	<81
57 Tau	27397	F0 IV	5.59	0.28	27874	6000	<38	<27
51 Eri	29391	F0 V	5.23	0.28	42307	2400	130:	67
8 Dra	112429	F0 V	5.24	0.28	33606	1440	140::	71
44 Oph	157792	A3m	4.17	0.28	30475	2640	<68	<13
HR 7160	175938	A8 V	6.39	0.28	23045	600	<86	<120
δ Ind	208450	F0 IV	4.40	0.28	32109	720	<200	<47
ϵ Cep	211336	F0 IV	4.19	0.28	32146	480	<140	<27
HR 1566	31236	F3 IV	6.37	0.29	27891	3600	<97	<140
υ UMa	84999	F2 IV	3.80	0.29	29565	2040	41::	5.6
					32104	360	<120	<17
β TrA	141891	F2 III	2.85	0.29	4184	120	810::	45
					30268[a]	25500	640::	36
53 Her	152598	F0-2 V	5.32	0.29	32999	1200	320::	170
					33609	1620	160:	87
7 And	219080	F0 V	4.52	0.29	10226	1200	110::	29
					32147	600	140::	36
γ Dor	27290	F4 III	4.25	0.30	7346	2399	110::	22
23 And	905	F0 IV	5.72	0.31	10366	4200	64::	50
59 Dra	180777	A9 V	5.13	0.31	28550	5400	250::	110
					33000	1200	<160	<71
					33607	1260	220:	100

Table 1 (continued)

Star	HD	Spectral Type	V	$B-V$	Image	Exposure (s)	f(Lyα) (10^{-14})	R(Lyα) (10^{-7})
76 Tau	28204	F0 IV	5.90	0.32	10247	2160	<77	<72
HR 2740	55892	F0 IV	4.49	0.32	28544	4200	180:	44
HR 4803	109709	F1 IV	5.45	0.32	37979	4500	<64	<39
16 Lib	132052	F0 V	4.49	0.32	28549	4200	160::	39
δ Hor	26612	A9 V	4.93	0.33	8213	240	<60	<23
η Lep	40136	F1 III	3.71	0.33	8190	60	390:	48
23 UMa	81937	F0 IV	5.67	0.33	37554	420	430:	51
S Ant	82610	A9 V	6.46	0.33	9400	7200	120::	180
HR 4191	92787	F5 III	5.18	0.33	37553	960	190::	91
β Crv	432	F2 III-IV	2.27	0.34	2373	390	860:	28
					10227	600	970:	32
					29124	300	1100:	36
					29125	300	1300:	41
					29126	300	1800::	57
					31589	660	1200:	38
16 Per	17584	F2 III	4.23	0.34	22376	2700	180:	36
σ Cae	29875	F2 V	4.45	0.34	2696	240	<140	<34
δ Gem	56986	F2 IV	3.53	0.34	18914	120	480:	50
37 UMa	91480	F1 V	5.16	0.34	15181	3600	270::	130
					32160	1500	180:	85
HR 7887	196629	F0 V	6.49	0.34	10468	3300	<42	<67
HR 4102	90589	F2 IV	4.00	0.35	29307	720	430:	69
26 Boo	127739	F2 IV	5.92	0.35	5131	1500	<140	<130
45 Tau	26462	F4 V	5.72	0.36	10204	3000	110::	89
γ Vir	110379	F0 V	3.65	0.36	19712	420	1430:	170
78 UMa	113139	F2 V	4.93	0.36	10210	1800	230:	87
					15178	4200	210::	80
σ Boo	128167	F2 V	4.46	0.36	6151	239	180:	45
					24568	3600	260:	63
HR 1354	27429	F3: V	6.12	0.37	10219	5400	82::	99
β Cae	29992	F1 V	5.05	0.37	7311	3300	47::	20
HR 4084	90089	F2 V	5.26	0.37	5134	2100	130:	67
HR 9028	223552	F3 V	6.44	0.37	14003	1020	160::	240
63 Gem	58728	F5 V + F5 V	5.22	0.38	20030	3000	320:	154
μ Vir	129502	F2 III	3.88	0.38	2659	780	470:	65
HR 6237	151613	F2 V	4.85	0.38	18915	1200	180::	64
θ Cyg	185395	F4 V	4.48	0.38	10202	300	<81	<20
HR 2530	49933	F2 V	5.77	0.39	8200	3000	93:	75
τ Cyg	202444	F2 IV	3.72	0.39	15739	2175	610:	75
					29128	1200	550:	68
78 Psc	6680	F5 IV	6.25	0.40	10469	3540	59::	84
κ Ret	22001	F5 IV-V	4.72	0.40	5097	1200	190::	57
48 Tau	26911	F5 V	6.32	0.40	10205	1800	61::	82
o Gem	61110	F3 III	4.90	0.40	21482	3600	210:	76
45 Oph	157919	F5 IV	4.29	0.40	36873	930	200::	42
ι Leo	99028	F4 IV	3.94	0.41	1631	600	390:	58
η Sco	155203	F3 III-IVp	3.33	0.41	2689	90	325:	28
					36875	1080	380::	32
ϵ CrA	175813	F2 V	4.87	0.41	9371	3300	450::	150
ρ And	1671	F5 III	5.18	0.42	23748	1410	110:	51
ω And	8799	F5 IV	4.83	0.42	14876	4200	210::	70
τ^6 Eri	23754	F3 III	4.23	0.42	10930	2700	66::	13
Procyon	61421	F5 IV-V	0.38	0.42	2826	60	5700:	32
					6660[a]	5400	6060::	34
					20048[a]	6600	6140::	34
					21198	120	5930	33
					22584	180	6150	34
ω Psc	224617	F4 IV	4.01	0.42	21775	2400	420:	67
HR 3220	68456	F5 V	4.76	0.43	16693	1800	130::	40
18 Com	108722	F5 III	5.48	0.43	20031	1800	230:	142
42 Aql	185124	F3 IV	5.46	0.43	21551	7200	143:	86
ψ Cap	197692	F4 V	4.14	0.43	10201	2100	510::	93
κ Peg	206901	F5 IV	4.13	0.43	18929	1200	290:	51
16 Cep	209369	F5 V	5.03	0.44	24287	3600	300::	122
ι Peg	210027	F5 V	3.76	0.44	10367	1800	218:	27

Table 1 (continued)

Star	HD	Spectral Type	V	$B-V$	Image	Exposure (s)	f(Lyα) (10^{-14})	R(Lyα) (10^{-7})
π^3 Ori	30652	F6 V	3.19	0.45	29306	720	620::	46
HR 3684	79940	F5 III	4.62	0.45	2694	1800	64::	18
					19737	900	310:	148
σ Com	114378	F5 V	5.22	0.45	19738	720	340:	164
					18650	3600	110::	70
50 Per	25998	F7 V	5.61	0.46	21478	1200	270:	19
θ UMa	82328	F6 IV	3.17	0.46	21552	3600	220:	41
110 Her	173667	F6 V	4.19	0.46	13790	3600	230:	24
					16624	1680	220:	23
γ Lep	38393	F6 V	3.60	0.47	14347	2100	800	590
					33820	1800	920	680
σ^2 CrB	146361	G0 V	5.64	0.47	24502	6000	200::	48
τ^1 Eri	17206	F6 V	4.47	0.48	6180	2999	150::	19
					10229	4080	200::	25
γ Ser	142860	F6 V	3.85	0.48	19999	2100	170:	59
19 Dra	153597	F6 V	4.89	0.48	6126	89	1700:	150
					24603	90	800::	72
					29304	600	1400:	130
α Tri	11443	F6 IV	3.41	0.49	35000*	24300	1700::	150
χ Dra	170153	F7 V	3.57	0.49	10225	1800	350:	36
γ Pav	203608	F6 V	4.22	0.49	7308	4199	160::	31
ρ Tuc	4089	F6 V	5.39	0.50	19025	1800	<92	<51
θ Boo	126660	F7 V	4.05	0.50	20636	1800	570::	94
ι Psc	222368	F7 V	4.13	0.51	7310	3599	150::	26
HR 784	16673	F6 V	5.78	0.52	16333	5400	78::	61
					14034	1860	320::	92
ζ Dor	33262	F7 V	4.72	0.52	19784	1860	240:	72
ι Vir	124850	F6 III	4.08	0.52	9464	3600	380:	62
θ Dra	144284	F8 IV	4.01	0.52	10881	2700	370:	57
99 Her	165908	F7 V	5.04	0.52	7767	1800	56::	22
					9683	2880	290:	110
111 Tau	35296	F8 V	4.99	0.53	16691	2100	340:	128
HR 7955	198084	F8 IV-V	4.51	0.54	10466	1800	52::	13
β Vir	102870	F9 V	3.61	0.55	7305	1799	270:	28
13 Cet	3196	F8 V	5.20	0.56	21784	2400	150:	67
HR 5534	130948	G0-2 V	5.85	0.56	24969	1800	220:	180
χ Her	142373	F8 V	4.62	0.56	26800	2400	70::	19
η Cas	4614	G0 V + dM0	3.44	0.57	7433	1319	160::	14
β Com	114710	G0 V	4.26	0.57	9465	3780	70::	13
ζ Tuc	1581	F9 V	4.23	0.58	16336	2400	120::	22
η Boo	121370	G0 IV	2.68	0.58	1487	1980	330::	15
					22221	1500	420:	91
χ Ori	39587	G0 V	4.41	0.59	22408	840	450:	97
β CVn	109358	G0 V	4.26	0.59	15717	3300	140:	27
HR 8314	206860	G0 V	5.94	0.59	23037	2400	68::	62
HR 3018	63077	G0 V	5.37	0.60	8211	900	130:	70
HR 3625	78366	F9 V	5.93	0.60	23040	2400	60::	52
δ Tri	13974	G0 V	4.87	0.61	15765	4200	220:	73
υ Peg	220657	F8 III	4.40	0.61	14001	2100	840:	180
					7429	719	340:	17
β Hyi	2151	G2 IV	2.80	0.62	16324	1200	350:	17
π^1 UMa	72905	G1.5 Vb	5.64	0.62	23039	2400	180:	130
ζ Her	150680	G0 IV	2.81	0.65	5731	719	390:	19
					8640	1500	110:	540
W UMa	83950	F8-G2	7.70	0.66	8654	5100	120:	580
31 Com	111812	G0 IIIp	4.94	0.67	7769	1200	1120:	400
44 Boo	133640	F9-G1 Vn	4.76	0.67	28569	900	1550:	1340
κ^1 Cet	20630	G5 V	4.83	0.68	34180	1980	470:	140
					34256	2700	680::	1700
EI Eri	26337	G5 IV + ?	7.10	0.68	34270	2700	500:	1260
35 Cnc	72779	G0 III	6.58	0.68	8794	3000	<39	<63
					17281	2700	<100	<63
ψ^3 Psc	6903	G0 III	5.55	0.69	17377	1800	56::	34
					24724	2400	470::	2800
FK Com	117555	pec	8.20	0.69	35884	1860	880:	5200

Table 1 (continued)

Star	HD	Spectral Type	V	$B-V$	Image	Exposure (s)	f(Lyα) (10^{-14})	R(Lyα) (10^{-7})
HR 1008	20794	G8 V	4.27	0.71	15909	3600	170::	32
					22583	1200	110:	20
					5540	119	4780	17.4
					13886	180	4930	17.9
α Cen A	128620	G2 V	−0.01	0.71	17007	180	4860	17.7
					17026	180	4930	17.9
					22599	120	5560	20.2
τ Cet	10700	G8 V	3.50	0.72	17535	1800	450	40
61 UMa	101501	G8 V	5.33	0.72	22005	3600	250:	120
κ Del	196755	G5 IV + K2 IV	5.05	0.72	13999	2400	39::	14
AR Lac	210334	G2 IV + K0 III	6.11	0.72	23858	1800	780:	650
					31083	1800	820:	680
ξ Boo A	131156	G8 V + K4 V	4.55	0.76	9532	1800	850::	210
					17525	1200	1250::	310
					26508*	44100	620::	160
					28525*	30000	580::	150
μ Her	161797	G5 IV	3.42	0.76	17537	1800	<210	<18
δ Pav	190248	G6-8 IV	3.56	0.76	2827	2400	190	17
					22600	1200	<130	<12
24 UMa	82210	G4 III-IV	4.56	0.77	8784	1800	680:	150
PZ Tel	174429	K0 IVp	8.50	0.77	28803	7200	76::	090
σ Dra	185144	K0 V	4.68	0.79	7048	1199	380:	95
Capella	34029	G5 IIIe + G0 III	0.08	0.80	13557	25	26800	99
					13700*	1800	35000::	130
					13808*	1800	30400::	112
					13820	24	29700	110
					28058*	2101	33300::	123
					28063*	2102	33900::	125
δ CrB	141714	G3.5 III-IV	4.63	0.80	14262	4380	350:	88
40 Eri A	26965	K1 V	4.43	0.82	26921	900	280:	54
β Lep	36079	G5 II	2.84	0.82	5753	899	310:	14
AB Dor	36705	K2 IVp	6.90	0.83	35077	1320	890:	1500
V491 Per	25893	G8 IV	7.13	0.85	33100	6600	190:	430
70 Oph A	165341	K0 V	4.03	0.86	10211	431	680:	91
					31483	1080	1020:	136
VW Cep	197433	G8	7.08	0.86	7866	3600	320:	670
					30713	3000	450:	940
ε And	3546	G8 IIIp	4.37	0.87	7766	1200	110::	20
HR 7703	191408	K3 V	5.32	0.87	22619	1800	130::	55
ε Eri	22049	K2 V	3.73	0.88	10094	720	2040	195
					17515	1200	2050:	196
					21192*	31800	1660::	158
					26466	720	1840:	176
					29439	720	1960	187
					29607	720	1710	164
α Cen B	128621	K1 V	1.33	0.88	16997	160	3570	38
ο Tau	21120	G6 III	3.60	0.89	24991	4800	160:	14
β CrV	109379	G5 II	2.65	0.89	1571	2700	150::	5.7
ε UMi	153751	G5 III	4.23	0.89	31724	2400	210:	33
AY Cet	7672	G5 IIIe + wd	5.41	0.90	21598	3600	420:	200
					21660	3600	290:	140
					21966	2700	340:	165
					22220	3600	270:	130
TW Lep	37847	G8 III + ?	7.00	0.90	29551	7200	110::	250
μ Vel	93497	G5 III + G2 V	2.69	0.90	2338	900	1560	59
LQ Hya	82558	dK0	7.50	0.91	34632	3000	150::	610
η Dra	148387	G8 III	2.74	0.91	1551	2700	260:	11
δ Eri	23249	K0+ IV	3.54	0.92	15019	3600	360:	29
26 Aql	181391	G8 III-IV	5.01	0.92	29553	1500	69::	22
η Cep	198149	K0 IV	3.43	0.92	7435	1799	390::	29
UX Ari	21242	G5.V + K0 IV	6.60	0.93	15211*	25200	1600::	2000
					15240*	24000	2000::	2500
HR 5110	118216	F2 IV + K2 IV	7.02	0.93	13669*	22680	2300::	4500
β Her	148856	G7 IIIa	2.77	0.94	5747	899	280::	12
ξ Her	163993	G8 III	3.70	0.94	7768	1200	380::	35
					14859	960	380:	35

Table 1 (continued)

Star	HD	Spectral Type	V	$B-V$	Image	Exposure (s)	f(Lyα) (10^{-14})	R(Lyα) (10^{-7})
θ^1 Tau	28307	K0 IIIb	3.84	0.95	19515	1200	350::	35
δ Boo	135722	G8 III	3.47	0.95	19851	2400	230:	17
VY Ari	17433	K3/4 IV	6.87	0.96	30282	2400	870:	1100
HR 9038	223778	K3 V	6.39	0.98	10959	3600	370::	370
HR 1099	22468	G5 IV + K1 IV	6.32	0.99	15163[a,b]	7200	13000::	13000
δ Lep	39364	G8 III	3.81	0.99	32531	2100	360::	35
β Gem	62509	K0 IIIb	1.14	1.00	7431	479	1300::	11
ζ Hya	76294	G9 II-III	3.11	1.00	8806	1800	200:	10
γ^2 Sgr	165135	K0 III	2.99	1.00	6832	1799	350::	16
ζ Cyg	202109	G8 III-IIIa	3.20	1.00	8801	1800	130	7.4
ζ Cap	204075	G8 III + wd	3.74	1.00	5307	4200	240::	24
β Cet	4128	K0 III	2.04	1.01	14786[a]	47700	2600::	50
θ Cen	123139	K0 IIIb	2.06	1.01	5089	600	440::	8.3
λ And	222107	G8 III-IV	3.82	1.01	18485[b]	180	3580	326
					18486[b]	180	3590	327
11 Peg	224085	K2-3 IV-V + ?	7.35	1.01	26448	900	580::	1340
					26456	1200	640:	1500
					26457	2400	720::	1670
γ Cep	222404	K1 III-IV	3.21	1.03	10357	1499	290:	16
HD 34198	34198	K0 III	7.10	1.04	18536	4500	120:	238
IL Hya	81410	K1 III	7.45	1.05	18520	3600	170::	450
ϵ Ind	209100	K4-5 V	4.69	1.06	13891	1440	550:	100
					22618	1200	640:	120
α UMa	95689	K0 IIIa	1.79	1.07	10914	600	1000:	14
α Phe	2261	K0 III	2.39	1.09	8804	2280	>770	>19
1 Gem	41116	G7 III + F6 IV	4.73	1.10	10883	4800	240::	50
HR 5568	131977	K4 V	5.74	1.11	22598	2400	200::	95
ζ And	4502	K1 IIa	4.06	1.12	26450	1200	>2600	>290
σ Gem	62044	K1 III	4.28	1.12	29306	360	4470	560
HR 8703	216489	K1-2 II-IIIe	5.72	1.12	26507	3000	170::	76
HR 4665	106677	K0 III + K0 III	6.29	1.14	1565	3600	230:	200
α Ari	12929	K2 III	2.00	1.15	9868	1500	>1120	>18
ϵ Sco	151680	K2.5 III	2.29	1.15	10362	1669	650::	10
κ Oph	153210	K2 III	3.20	1.15	10359	1545	160::	7.7
HR 1927	37434	K2 III	6.11	1.16	30734	5400	140::	96
β Oph	161096	K2 III	2.77	1.16	6574	1800	100:	3.4
					10360	2400	200::	6.6
α Cas	3712	K0 IIIa	2.23	1.17	10358	1499	96:	2.1
α Ser	140573	K2 III	2.65	1.17	8800	2044	460::	14
ξ Dra	163588	K2 III	3.75	1.18	8721	900	250::	20
61 Cyg A	201091	K5 V	5.21	1.18	10014	1800	530:	136
					10091	1800	540:	138
					10739	720	590::	150
HR 454	9746	gK1	5.92	1.21	29133	5100	<42	<24
BY Dra	234677	dK5e + dK7e	8.07	1.22	15157	3600	180::	390
α Boo	124897	K1 III	−0.04	1.23	4233[a]	7200	12200::	25
					33062	140	13700	28
ν Hya	93813	K2 III	3.11	1.25	25876	1500	290::	12
δ And	3627	K3 III	3.27	1.28	26414	1500	190::	8.6
51 And	9927	K3- III	3.57	1.28	18933	1800	120::	7.2
Gl 900	...	dM0.5e	9.56	1.35	34664	1800	<100	<1000
Gl 380	88230	dK7	6.59	1.36	35359	1800	450:	325
AX Mic	202560	M0 V	6.67	1.38	29200	1800	260::	180
α Tuc	211416	K3 III	2.86	1.39	8803	1980	460:	12
ν UMa	98262	K3 III	3.48	1.40	25875	1500	290::	13
Gl 784	191849	dM1	7.95	1.41	29102	2220	120::	250
α Hya	81797	K3 II-III	1.98	1.44	31126[a]	57000	900::	9.4
α TrA	150798	K2 IIb-IIIa	1.92	1.44	28040	900	1050:	10
DT Vir	...	dM1.5e	9.78	1.46	30277	1500	130:	880
AU Mic	197481	M1.6 Ve	8.60	1.47	6428	1800	280::	1070
					21520	1800	520::	2000
					28374	1800	240:	920
					29279	1200	570:	2200
β Cnc	69267	K4 III	3.52	1.48	25877	1500	300::	12
YY Gem	...	dM1.5e	9.07	1.49	33053	1500	240:	1100
FK Aqr	214479	M0 Vpe	9.10	1.49	26983	3300	330:	1200

Table 1 (continued)

Star	HD	Spectral Type	V	$B-V$	Image	Exposure (s)	f(Lyα) (10^{-14})	R(Lyα) (10^{-7})
Gl 887	217987	M2 V	7.36	1.49	32126	1800	220:	220
V1396 Cyg	...	dM3e	10.28	1.50	18710	3600	110::	1200
σ Oph	157999	K2 II	4.34	1.50	9648	1440	<65	<5.9
σ Pup	59717	K5 III	3.25	1.51	26419	1500	550:	16
Gl 411	95735	M2 Ve	7.48	1.51	35337	1800	180:	150
γ Aql	186791	K3 II	2.72	1.52	7335	1500	240:	4.2
V1285 Aql	...	dM2e	10.11	1.53	15176	2040	120::	1100
AD Leo	...	dM3.5e	9.37	1.54	19172	2100	160::	550
					25668	3360	360::	1240
α Tau	29139	K5 III	0.85	1.54	3380[a]	8400	6500::	18
η Sgr	167618	M3.5 III	3.11	1.56	25884	1500	570:	5.8
ϕ Aqr	219215	M1.5 III	4.22	1.56	34611	3600	180:	10
γ Phe	9053	M0- IIIa	3.41	1.57	26418	1500	>1600	>45
55 Peg	218329	M1 IIIab	4.52	1.57	34612	3600	<31	<2.4
β And	6860	M0 IIIa	2.06	1.58	5845	899	2120	18
δ Vir	112300	M3 III	3.38	1.58	26421	1500	780	11
γ Eri	25025	M0.5 III	2.95	1.59	26415	1500	680:	12
μ UMa	89758	M0 III	3.05	1.59	8215	2400	>2500	>48
γ Cru	108903	M3.5 III	1.63	1.59	24892[a]	47700	2500::	5.0
AT Mic	196982	dM4.5e	10.83	1.59	19690	1200	300::	1400
					19691	960	320::	1500
					21521	1500	440:	2000
					26672[a]	59940	640::	2900
EV Lac	...	dM4.5e	10.10	1.60	14884	1800	580:	3400
					21372	4800	160:	970
β Gru	214952	M5 III	2.10	1.60	5846	359	630:	1.4
YZ CMi	...	dM4.5e	11.18	1.60	6861	2999	120:	1350
V1216 Sgr	...	dM4.5e	10.60	1.61	32120	1800	140:	1070
V998 Ori	...	dM4e	11.50	1.62	32127	1500	100::	1500
τ^4 Eri	20720	M3.5 III	3.69	1.62	27234	1800	240:	3.8
Wolf 630	152751	dM3.5e	9.40	1.62	9794	2160	280:	680
β Peg	217906	M2.5 II-III	2.42	1.67	14211	1380	470:	2.9
YZ Cet	...	dM5e	12.05	1.84	32333	1800	<99	<1700
UV Cet	...	dM6e + dM5.5e	12.70	1.85	18690	1800	160::	3200
					21233	1200	200:	4000
Prox Cen	...	dM5.5e	11.05	1.97	9847[b]	3600	330:	1050
					9848	3840	230::	740

[a] High dispersion.
[b] Spectrum during flare outburst.

Table 2: Intrinsic Lyman Alpha Fluxes

Star	HD	B-V	Atten[a]	f(Lyα)[b]	Qual[c]
δ^2 Tau	27819	0.15	0.49	<290	
80 UMa	116842	0.16	0.44	<570	
ι UMa	76644	0.19	0.42	<3600	
γ Boo	127762	0.19	0.61	<410	
α Aql	187642	0.22	0.31[d]	7600	c
22 Boo	126661	0.23	0.52	<170	
38 Ari	17093	0.24	0.44	<175	
45 Ori	37077	0.24	0.44	<230	
49 UMa	95310	0.24	0.57	<150	
κ^2 Tau	27946	0.25	0.47	94	c
HR 1507	30034	0.25	0.43	100	c
30 LMi	90277	0.25	0.56	110	c
HR 3350	71935	0.25	0.49	<110	
HR 4086	90132	0.25	0.47	<100	
υ Tau	28024	0.26	0.46	<300	
83 Tau	28556	0.26	0.44	<410	
HR 1480	29499	0.26	0.43	<120	
64 Eri	32045	0.26	0.51	<130	
η Hor	16555	0.27	0.44	<80	
15 UMa	78209	0.27	0.40	<180	
14 Com	108283	0.27	0.56	<80	
α Hyi	12311	0.28	0.52	240	b
51 Tau	27176	0.28	0.45	<240	
57 Tau	27397	0.28	0.44	<90	
51 Eri	29391	0.28	0.33	400	b
8 Dra	112429	0.28	0.41	340	c
υ UMa	84999	0.29	0.48	90	c
γ Dor	27290	0.30	0.37	290	c
76 Tau	28294	0.32	0.42	<190	
HR 2740	55892	0.32	0.39	450	b
η Lep	40136	0.33	0.41	970	b
23 UMa	81937	0.33	0.49	880	b
HR 4191	92787	0.33	0.48	400	c
16 Per	17584	0.34	0.53	340	b
α Cae	29875	0.34	0.41	<340	
δ Gem	56986	0.34	0.43	1100	b
37 UMa	91480	0.34	0.39	470	b
26 Boo	127739	0.35	0.45	<310	
45 Tau	26462	0.36	0.37	310	c
γ Vir	110379	0.36	0.33	4300	b

Table 2: Intrinsic Lyman Alpha Fluxes (Cont.)

Star	HD	B-V	Atten	f (Lyα)	Qual
78 UMa	113139	0.36	0.42	550	b
σ Boo	128167	0.36	0.34	750	b
β Cae	29992	0.37	0.31	150	c
HR 4084	90089	0.37	0.34	390	b
63 Gem	58728	0.38	0.36	880	b
HR 2530	49933	0.39	0.36	260	b
78 Psc	6680	0.40	0.39	148	c
κ Ret	22001	0.40	0.33	560	c
48 Tau	26911	0.40	0.38	160	c
o Gem	61110	0.40	0.50	420	b
ι Leo	99028	0.41	0.42	920	b
Ome And	8799	0.42	0.45	470	c
τ^6 Eri	23754	0.42	0.38	180	c
Procyon	61421	0.42	0.42	14800	a
HR 3220	68456	0.43	0.35	360	c
18 Com	108722	0.43	0.51	450	b
π^3 Ori	30652	0.45	0.32	2000	c
HR 3684	79940	0.45	0.33	190	a
α Com	114378	0.45	0.31	1100	c
50 Per	25998	0.46	0.31	370	c
θ UMa	82328	0.46	0.48	550	b
γ Lep	38393	0.47	0.31	720	b
τ^1 Eri	17206	0.48	0.33	620	c
α Tri	11443	0.49	0.45	3800	b
χ Dra	170153	0.49	0.36	980	b
θ Boo	126660	0.50	0.36	1600	c
HR 784	16673	0.52	0.30	260	c
ζ Dor	33262	0.52	0.27	890	b
ι Vir	124850	0.52	0.45	840	b
111 Tau	35296	0.53	0.30	960	b
β Vir	102870	0.55	0.33	810	b
HR 5534	130948	0.56	0.24	890	c
χ Her	142373	0.56	0.37	190	c
η Cas	4614	0.57	0.26	600	c
β Com	114710	0.57	0.27	260	c
η Boo	121370	0.58	0.40	820	c
χ Ori	39587	0.59	0.29	1450	b
β CVn	109358	0.59	0.27	540	b
HR 3018	63077	0.60	0.46	300	b
HR 3625	78366	0.60	0.27	220	c

Table 2: Intrinsic Lyman Alpha Fluxes (Cont.)

Star	HD	B–V	Atten	f (Lyα)	Qual
δ Tri	13974	0.61	0.24	910	c
π^1 UMa	72905	0.62	0.23	780	c
ζ Her	150680	0.65	0.41	950	b
W UMa	83950	0.66	0.32	360	b
31 Com	111812	0.67	0.57	2000	b
44 Boo	133640	0.67	0.26	5900	b
κ^1 Cet	20630	0.68	0.23	2100	c
ψ^3 Psc	6903	0.69	0.37	150	c
FK Com	117555	0.69	0.53	1700	c
HR 1008	20794	0.71	0.40	280	b
α Cen A	128620	0.71	0.47[e]	10500	a
τ Cet	10700	0.72	0.21	2200	c
61 UMa	101501	0.72	0.19	1300	c
ξ Boo A	131156	0.76	0.23	3700	c
μ Her	161797	0.76	0.34	<620	
24 UMa	82210	0.77	0.42	1640	b
σ Dra	185144	0.79	0.28	1300	b
Capella	34029	0.80	0.61[f]	49000	b
δ CrB	141714	0.80	0.49	720	b
40 Eri A	26965	0.82	0.34	810	b
β Lep	36079	0.82	0.65	470	b
AB Dor	36705	0.83	0.19	4600	c
V491 Per	25893	0.85	0.21	910	c
70 Oph A	165341	0.86	0.23	4500	c
ϵ And	3546	0.87	0.51	220	c
ϵ Eri	22049	0.88	0.19	10800	b
α Cen B	128621	0.88	0.39[e]	9200	b
o Tau	21120	0.89	0.59	270	b
μ Vel	93497	0.90	0.65	2400	b
LQ Hya	82558	0.91	0.19	810	d
δ Eri	23249	0.92	0.33	1100	c
HR 5110	118216	0.93	0.34	6700	c
θ^1 Tau	28307	0.95	0.49	730	c
δ Boo	135722	0.95	0.55	410	b
VY Ari	17433	0.96	0.19	4600	d
HR 1099	22468	0.99	0.35	37000	c
δ Lep	39364	0.99	0.58	620	c
β Gem	62509	1.00	0.54	2400	b
ζ Hya	76294	1.00	0.55	370	b
λ And	222107	1.01	0.26[g]	14000	c

Table 2: Intrinsic Lyman Alpha Fluxes (Cont.)

Star	HD	B-V	Atten	f (Lyα)	Qual
ϵ Ind	209100	1.06	0.23	2400	c
α Uma	95689	1.07	0.63	1600	b
1 Gem	41116	1.10	0.45	540	c
61 Cyg A	201091	1.18	0.26	2050	c
α Boo	124897	1.23	0.63	21900	a
ν Hya	93813	1.25	0.59	500	c
δ And	3627	1.28	0.58	330	c
51 And	9927	1.28	0.60	200	c
GL 380	88230	1.36	0.21	2100	c
AX Mic	202560	1.38	0.27	980	c
ν Uma	98262	1.40	0.61	480	c
α Hya	81797	1.44	0.69	1300	c
DT Vir	...	1.46	0.19	700	d
YY Gem	...	1.49	0.20	1200	d
GL 887	217987	1.49	0.21	1000	d
σ Pup	59717	1.51	0.62	880	b
GL 411	95735	1.51	0.44	410	c
AD Leo	...	1.54	0.19	820	d
α Tau	29139	1.54	0.65	10000	c
β And	6860	1.58	0.58	3680	a
δ Vir	112300	1.58	0.60	1300	b
γ Eri	25025	1.59	0.62	1080	b
EV Lac	...	1.60	0.20	2900	d
YZ CMi	...	1.60	0.20	620	d
V1216 Sgr	...	1.61	0.21	670	d
V998 Ori	...	1.62	0.19	550	d
YZ Cet	...	1.84	0.22	<440	
UV Cet	...	1.85	0.23	880	c
Prox Cen	...	1.97	0.39[e]	840	c

[a]Factor by which Lyα flux is attenuated according to the LISM model discussed in the text

[b]Unattenuated Lyα flux $\times 10^{-14}$ cm^{-2} s^{-1} Å^{-1}

[c]Quality index a ($\pm$20%), b ($\pm$40%), c ($\pm$60%), d ($\pm$80% or worse)

[d]Used N(H I) = 3×10^{18} cm^{-2}, b(H I) = 13 km s^{-1}

[e]Used N(H I) = 5×10^{17} cm^{-2}, b(H I) = 14 km s^{-1}

[f]Used N(H I) = 1.9×10^{18} cm^{-2}

[g]Used N(H I) = 4×10^{18} cm^{-2}

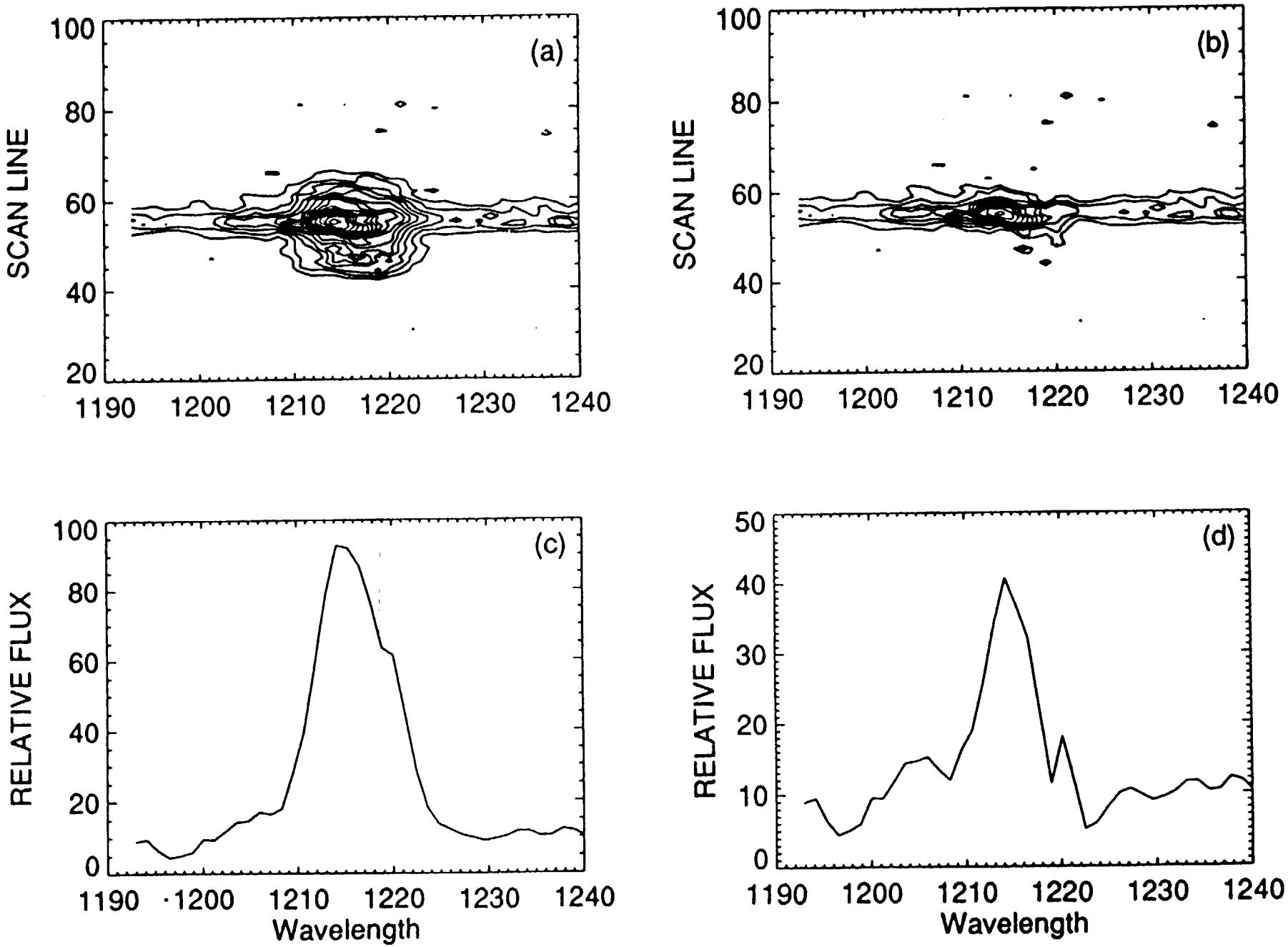
(a)
(b)
(c)
(d)
SCAN LINE
SCAN LINE
RELATIVE FLUX
RELATIVE FLUX
Wavelength
Wavelength
100
80
60
40
20
0
50
30
10
1190
1200
1210
1220
1230
1240

Figure 1

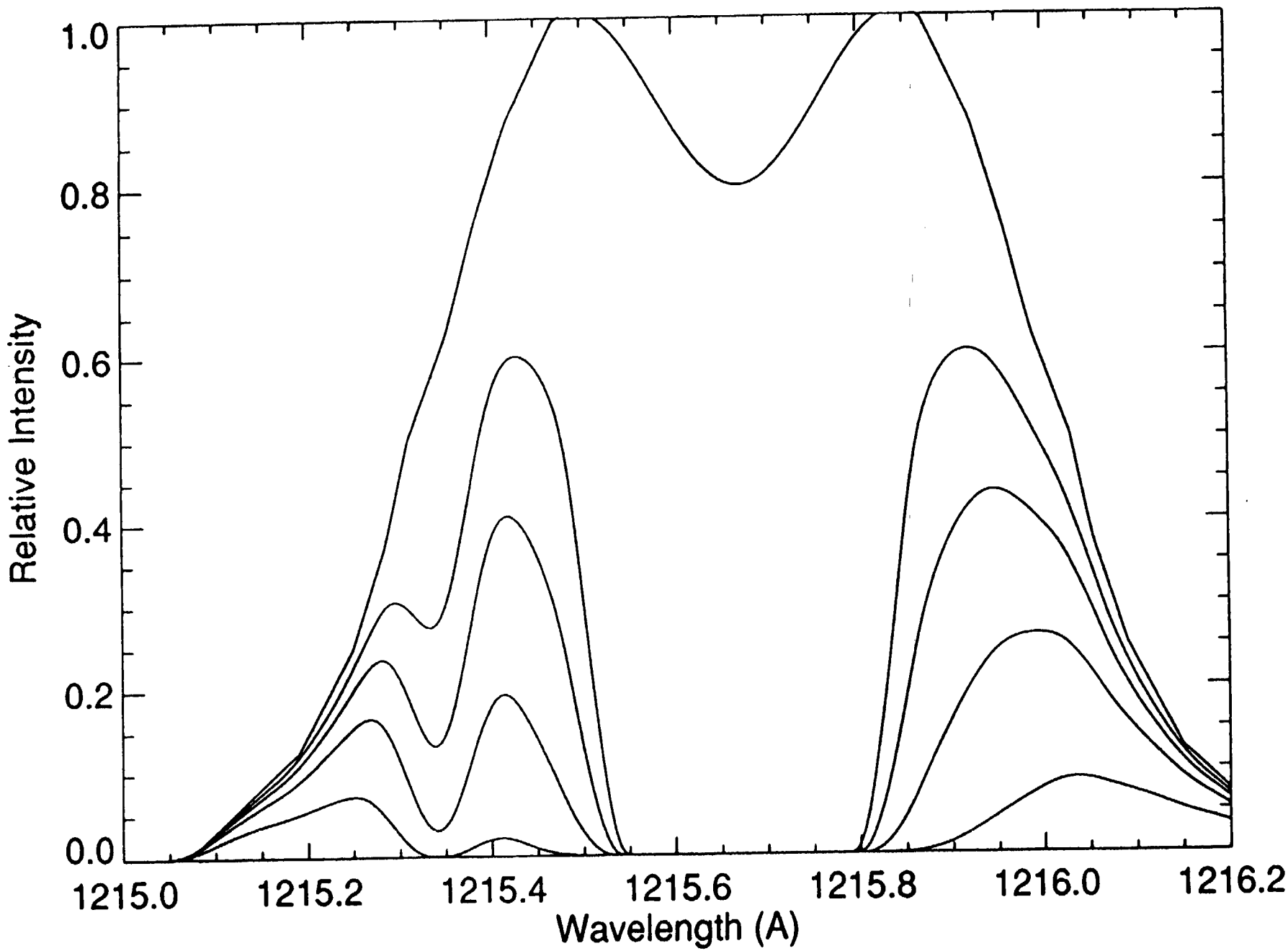
1.0
0.8
0.6
0.4
0.2
0.0
Relative Intensity
1215.0
1215.2
1215.4
1215.6
1215.8
1216.0
1216.2
Wavelength (A)

Figure 2

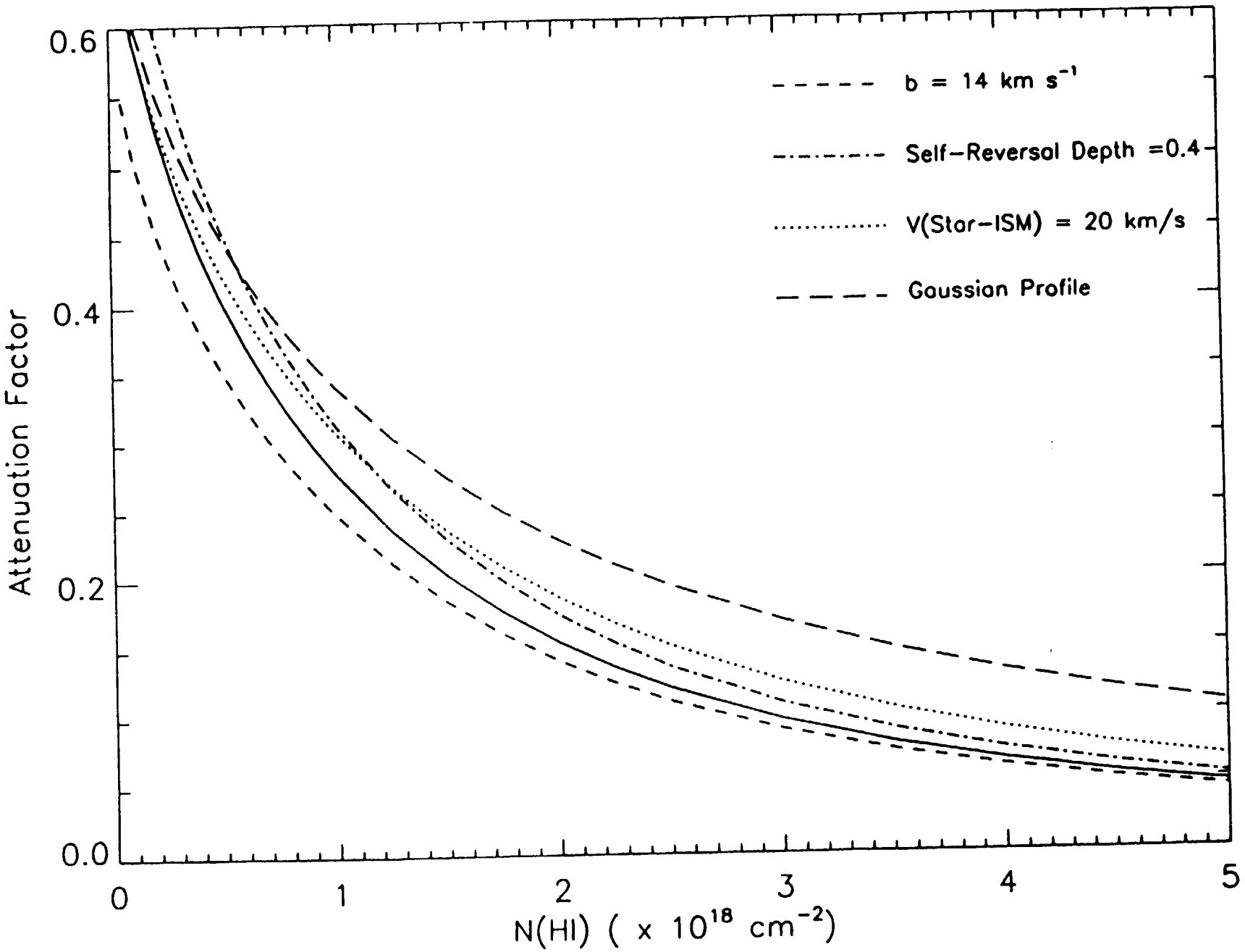
0.6
0.4
0.2
0.0
Attenuation Factor
0
1
2
3
4
5
N(HI) (x 10^18 cm^-2)
b = 14 km s^-1
Self-Reversal Depth =0.4
V(Star-ISM) = 20 km/s
Goussian Profile

Figure 3

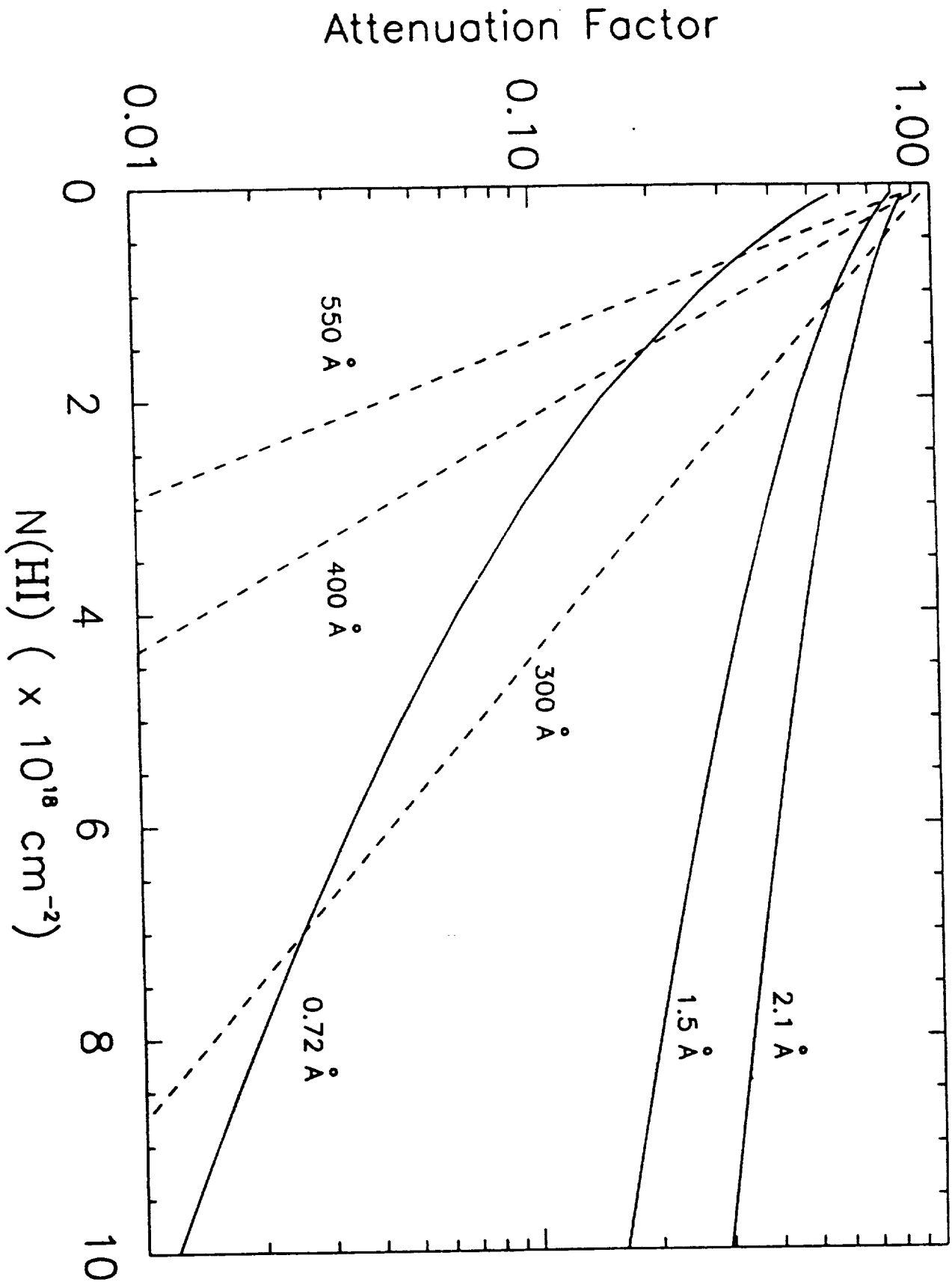
Attenuation Factor
1.00
0.10
0.01
0
2
4
6
8
10
N(HI) (x 10^18 cm^-2)
550 Å
400 Å
300 Å
0.72 Å
1.5 Å
2.1 Å

Figure 4

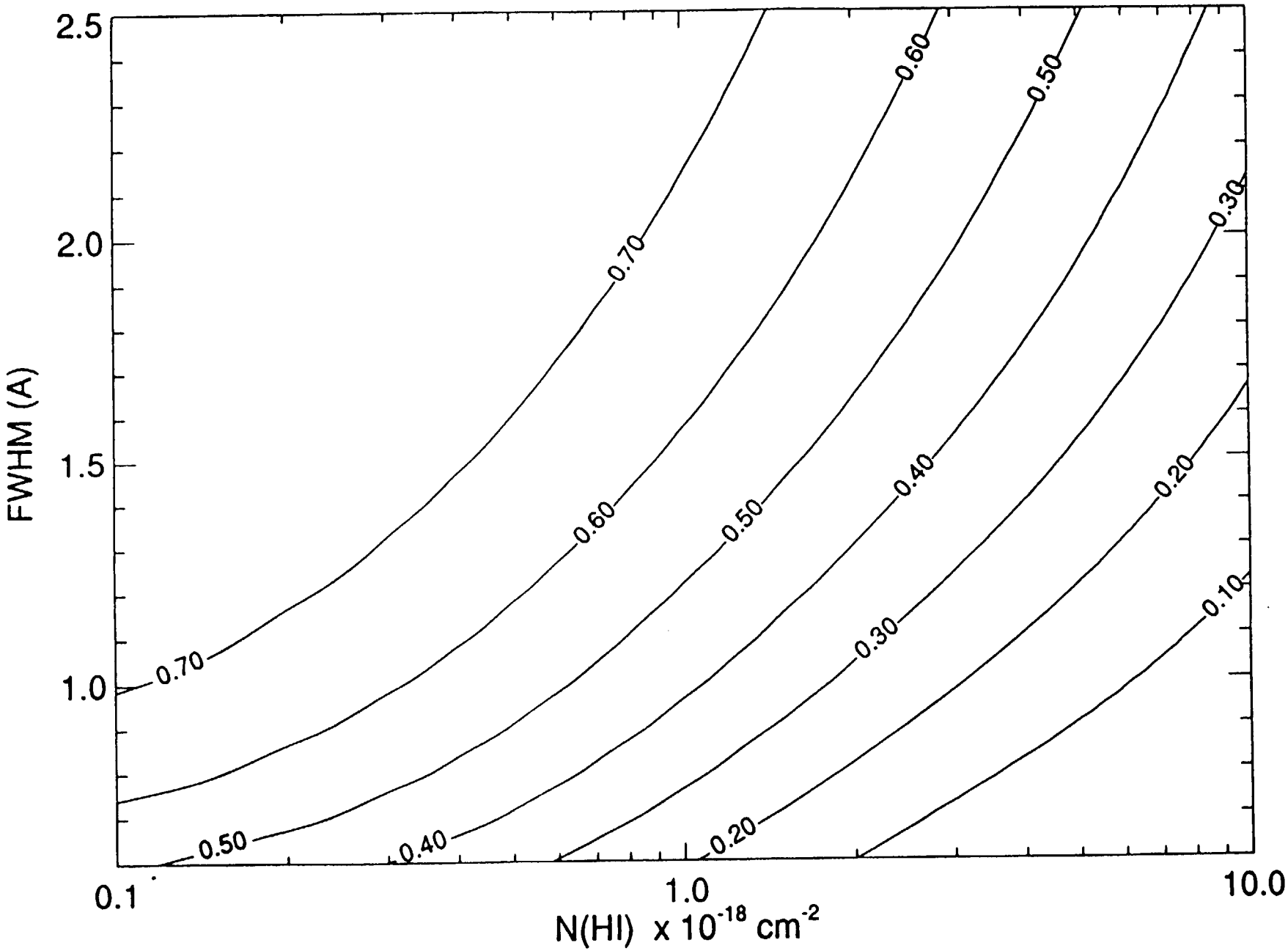
2.5
2.0
1.5
1.0
FWHM (A)
0.1
1.0
10.0
N(HI) x 10^-18 cm^-2
0.70
0.60
0.50
0.40
0.30
0.20
0.10

Figure 5

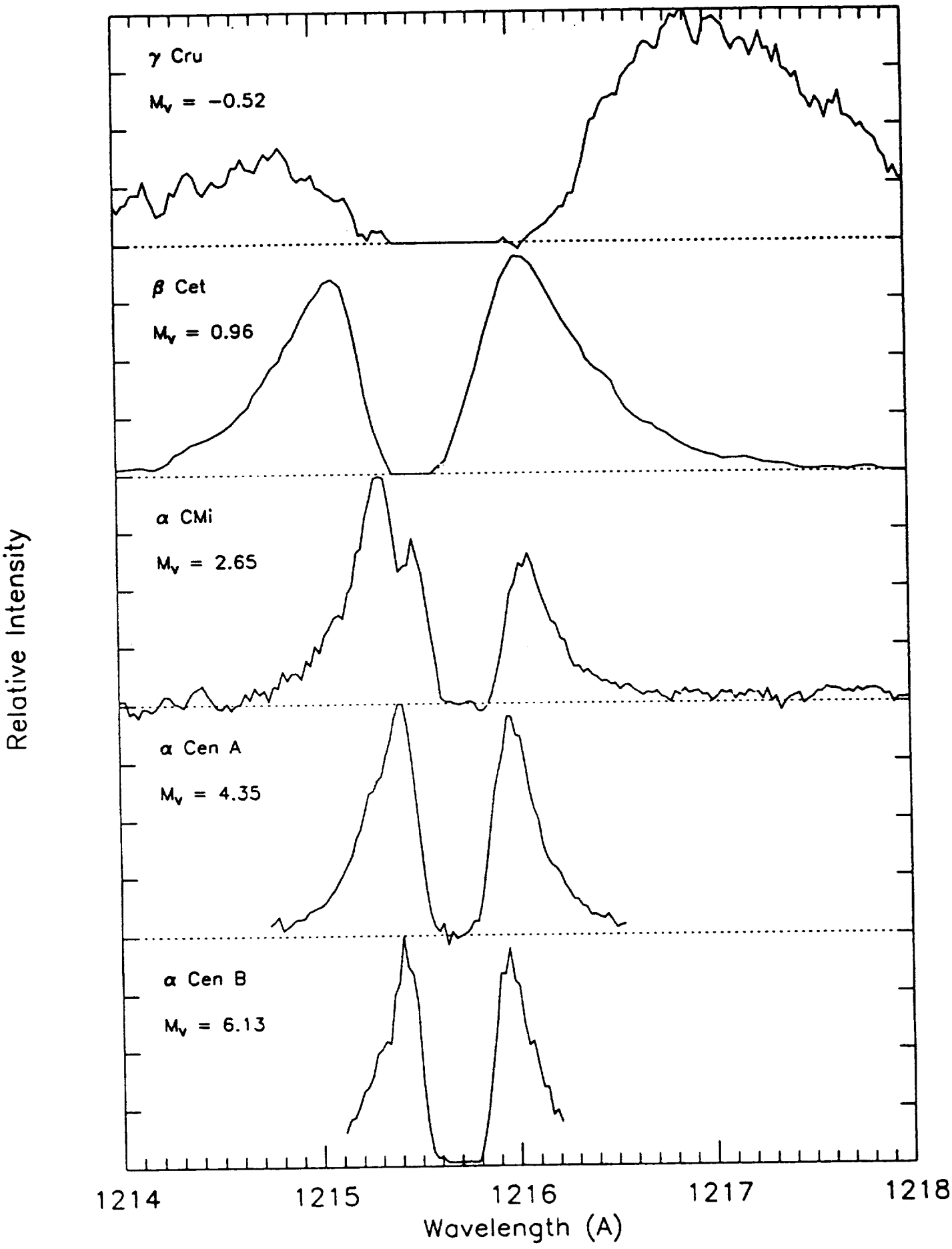
γ Cru
M_V = −0.52
β Cet
M_V = 0.96
α CMi
M_V = 2.65
α Cen A
M_V = 4.35
α Cen B
M_V = 6.13
Relative Intensity
1214
1215
1216
1217
1218
Wavelength (A)

Figure 6

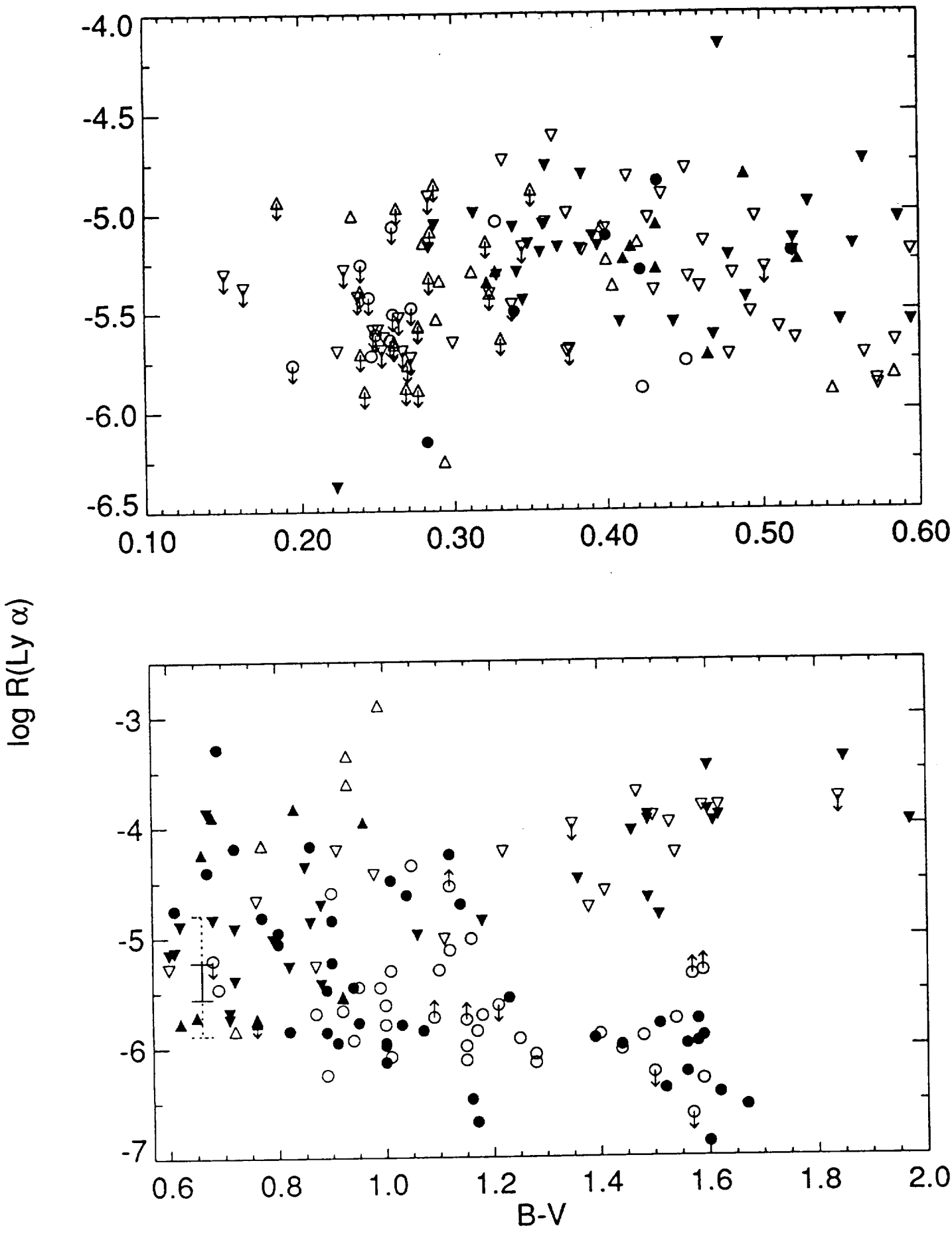
-4.0
-4.5
-5.0
-5.5
-6.0
-6.5
0.10
0.20
0.30
0.40
0.50
0.60
log R(Ly α)
-3
-4
-5
-6
-7
0.6
0.8
1.0
1.2
1.4
1.6
1.8
2.0
B-V

Figure 7

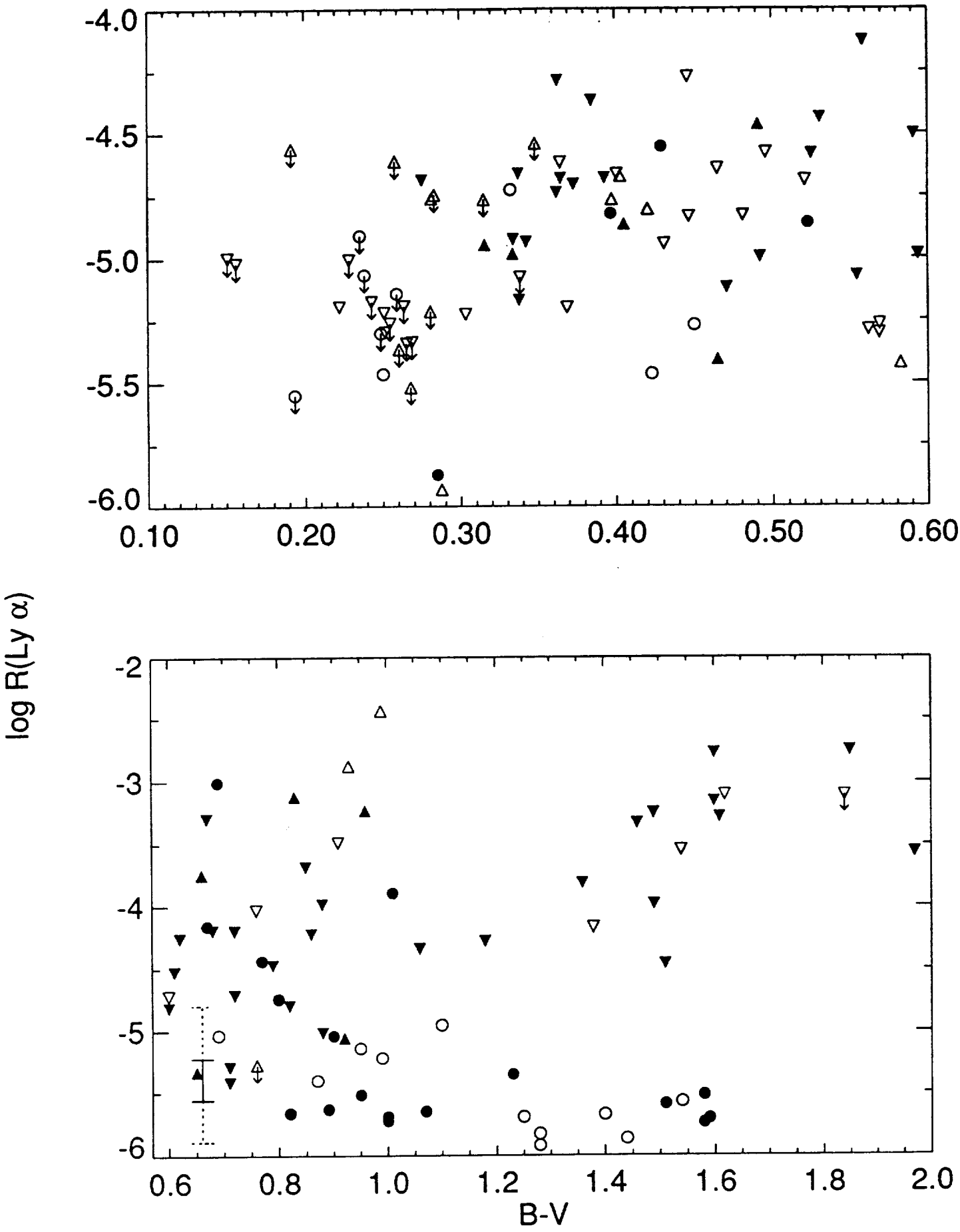
-4.0
-4.5
-5.0
-5.5
-6.0
0.10
0.20
0.30
0.40
0.50
0.60
log R(Ly α)
-2
-3
-4
-5
-6
0.6
0.8
1.0
1.2
1.4
1.6
1.8
2.0
B-V

Figure 8

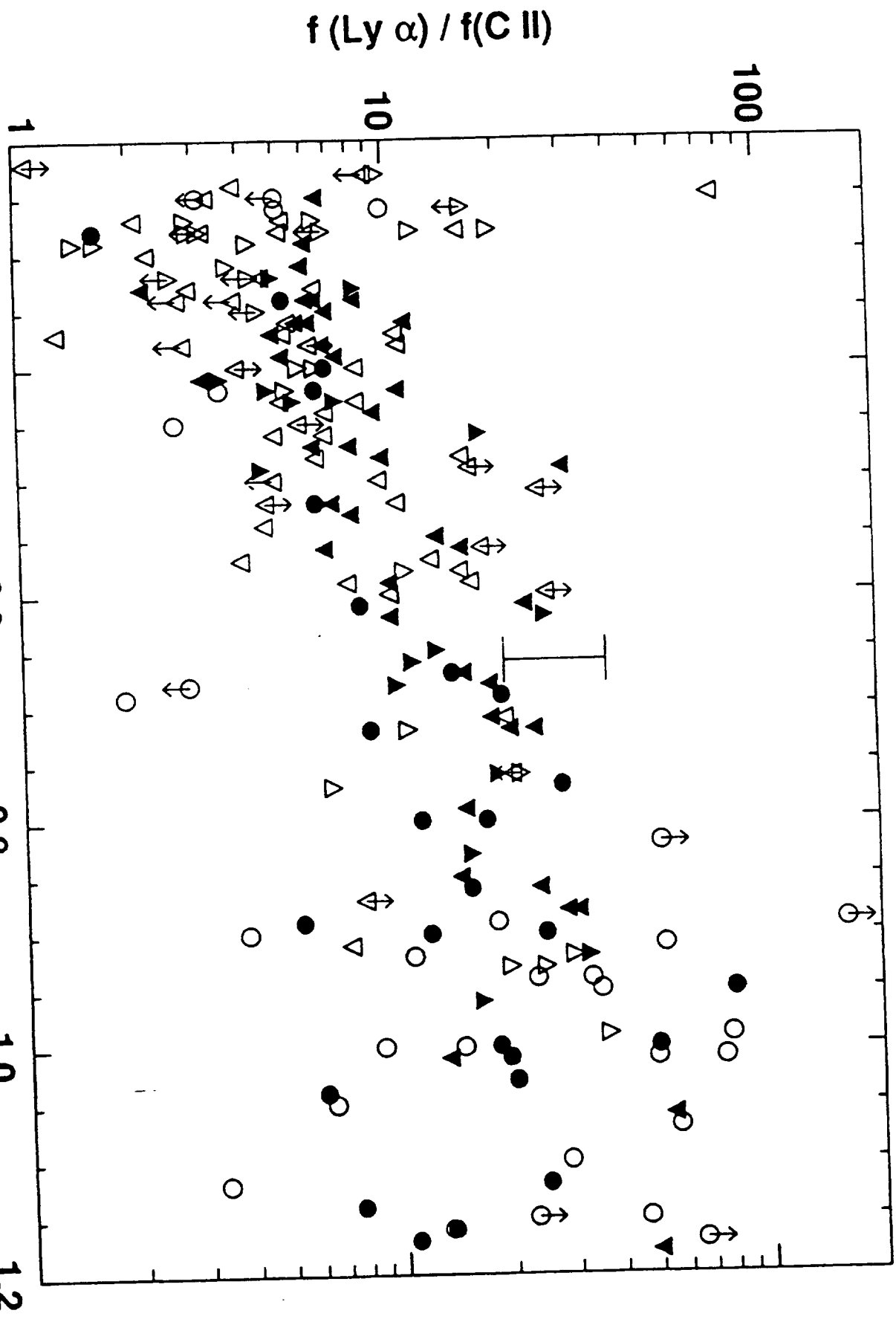

Figure 9

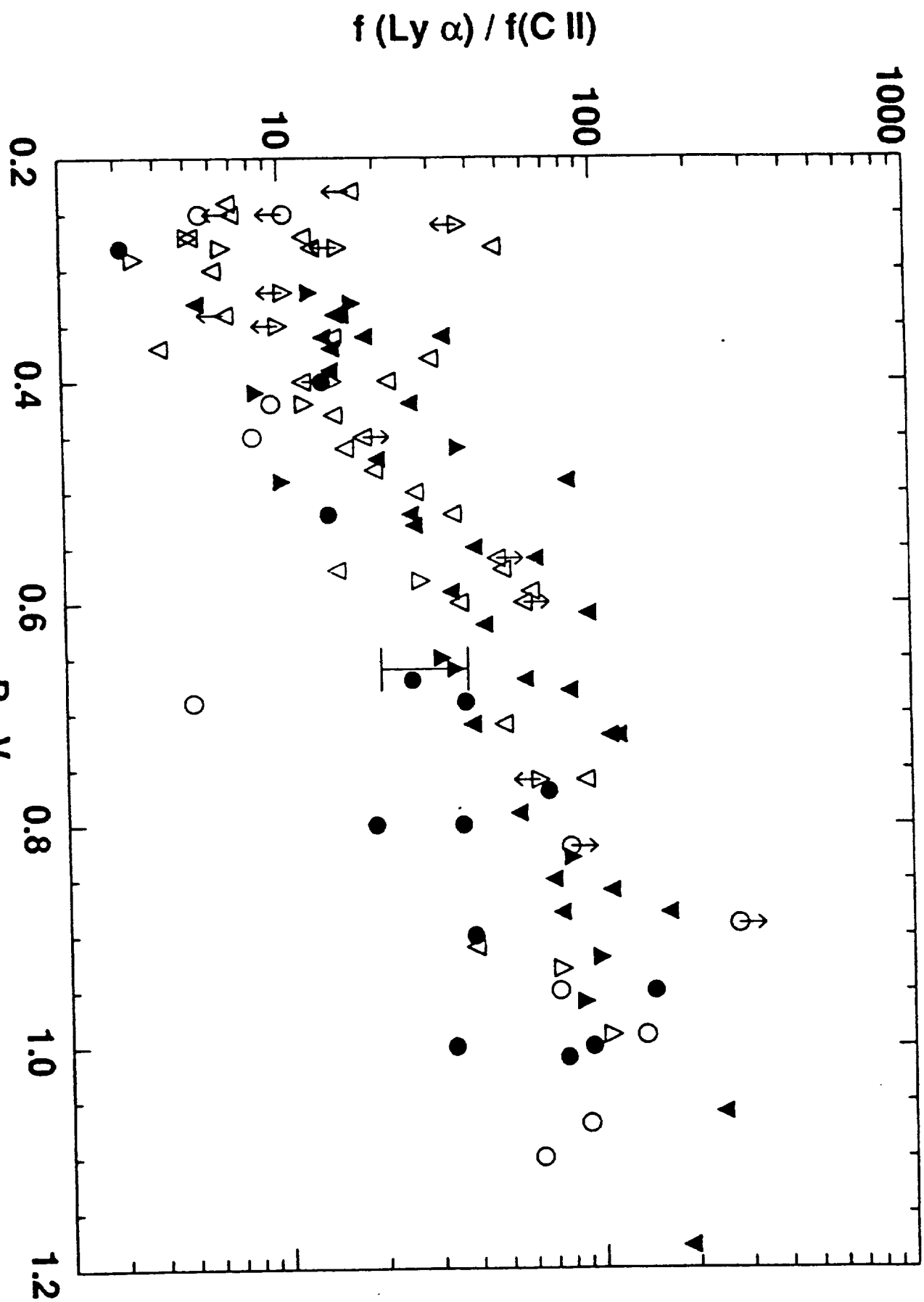

Figure 10

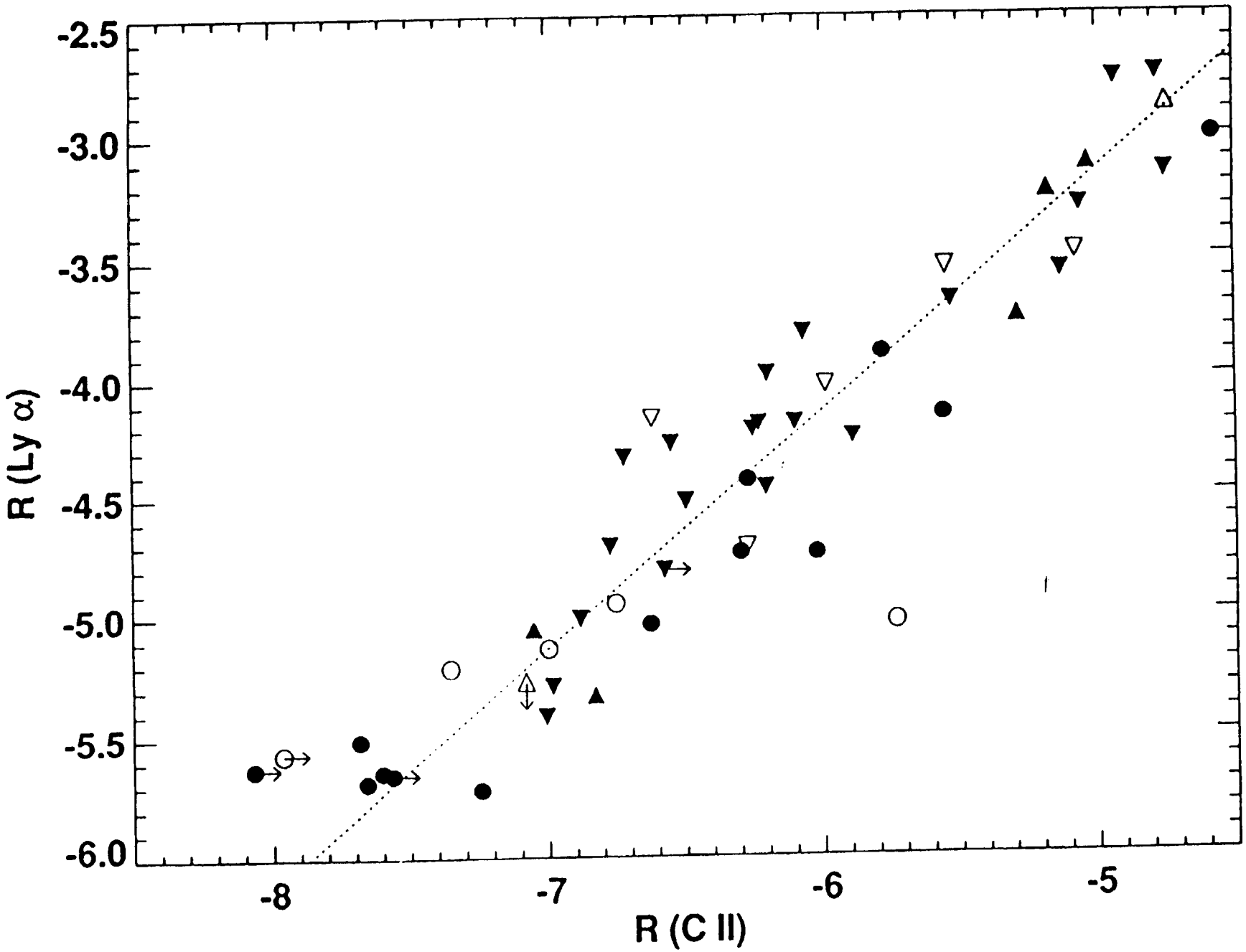

Figure 11

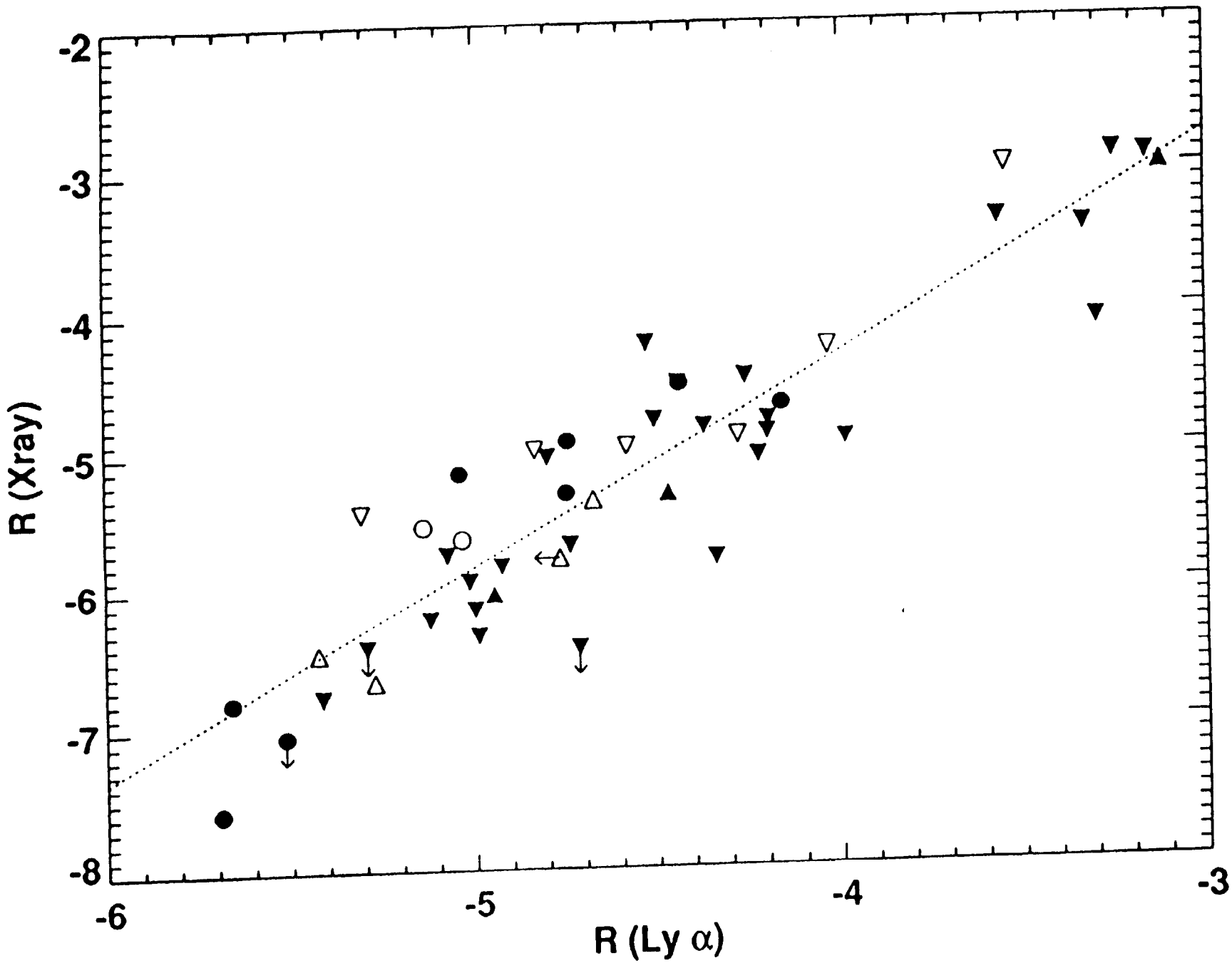

Figure 12

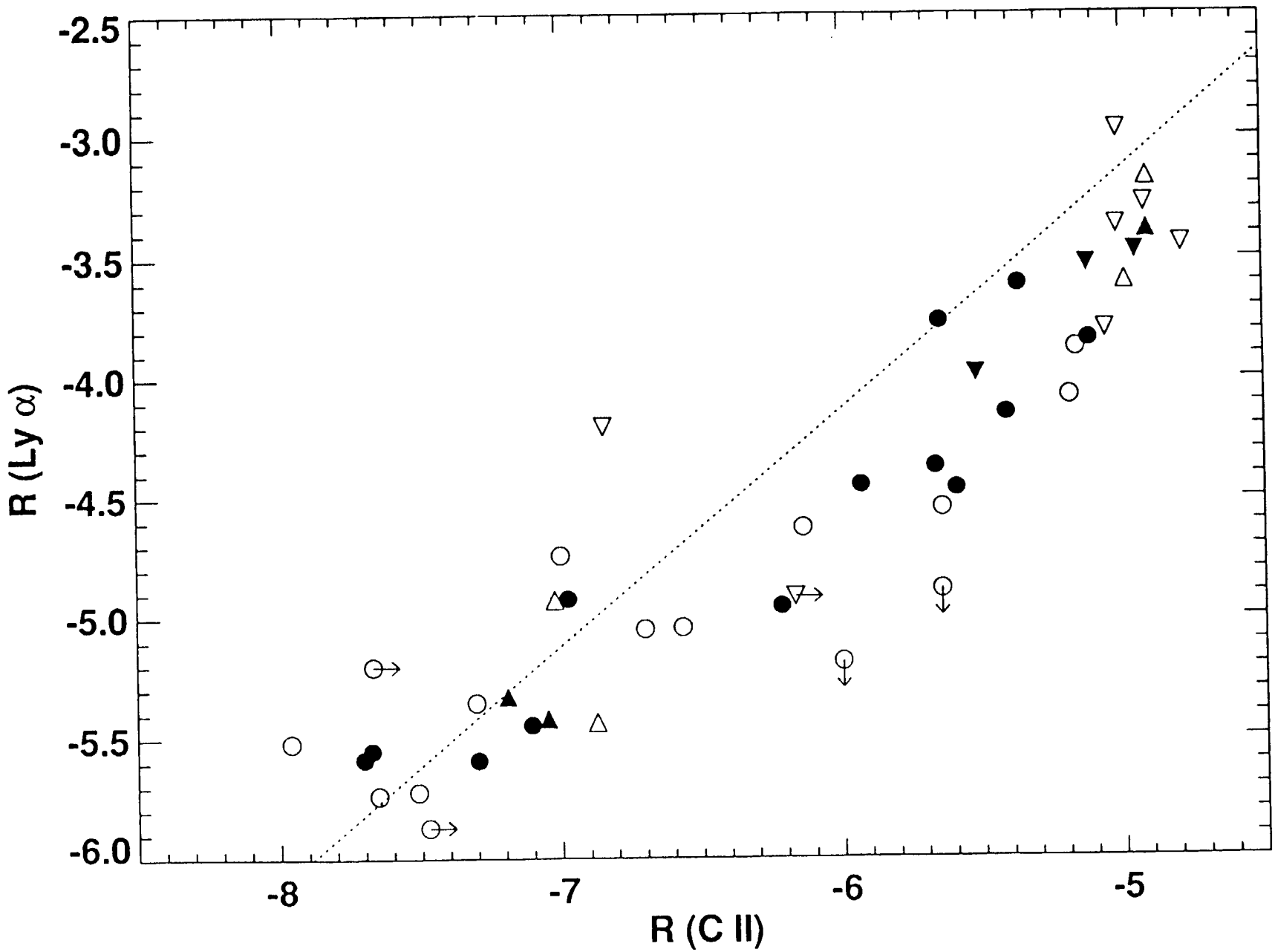

Figure 13